ARTICLE

Developmental regulation of an organelle tether coordinates mitochondrial remodeling in meiosis

Eric M. Sawyer[1] , Pallavi R. Joshi[1], Victoria Jorgensen[1] , Julius Yunus[2], Luke E. Berchowitz[2] , and Elçin Ünal[1]

Cellular differentiation involves remodeling cellular architecture to transform one cell type to another. By investigating mitochondrial dynamics during meiotic differentiation in budding yeast, we sought to understand how organelle morphogenesis is developmentally controlled in a system where regulators of differentiation and organelle architecture are known, but the interface between them remains unexplored. We analyzed the regulation of mitochondrial detachment from the cell cortex, a known meiotic alteration to mitochondrial morphology. We found that mitochondrial detachment is enabled by the programmed destruction of the mitochondria–endoplasmic reticulum–cortex anchor (MECA), an organelle tether that bridges mitochondria and the plasma membrane. MECA regulation is governed by a meiotic transcription factor, Ndt80, which promotes the activation of a conserved kinase, Ime2. We further present evidence for Ime2-dependent phosphorylation and degradation of MECA in a temporally controlled manner. Our study defines a key mechanism that coordinates mitochondrial morphogenesis with the landmark events of meiosis and demonstrates that cells can developmentally regulate tethering to induce organelle remodeling.

Introduction

Mitochondria are essential organelles that host an array of cellular processes, ranging from ATP production to iron–sulfur cluster assembly. In many cell types, mitochondria are organized into a network of interconnected tubules that is dynamically remodeled by fusion and fission (Friedman and Nunnari, 2014). In addition, the position and motility of mitochondria are regulated to allow proper distribution within the cell and inheritance during cell division (Mishra and Chan, 2014; Westermann, 2014). Although the list of factors that modulate mitochondrial architecture and dynamics continues to expand, relatively little is known about their developmental regulation.

Fusion, fission, anchoring, and transport collectively shape the mitochondrial network. All of these processes are broadly conserved in eukaryotes but have been most extensively characterized in *Saccharomyces cerevisiae*. The budding yeast mitochondrial network exists as a branched structure that is dynamically remodeled by fusion and fission, while maintaining associations with the plasma membrane (Hoffmann and Avers, 1973; Nunnari et al., 1997). Plasma membrane anchoring requires a protein complex called the mitochondria–ER–cortex anchor (MECA; Cerveny et al., 2007; Klecker et al., 2013; Lackner et al., 2013; Ping et al., 2016). MECA belongs to a growing list of protein complexes collectively known as tethers, which establish mem-

brane contact sites between disparate organelles (Kornmann et al., 2009; Elbaz-Alon et al., 2014, 2015; Murley et al., 2015; Murley and Nunnari, 2016). By physically bridging organelles, tethers enable interorganelle communication and establish spatial cellular organization (Eisenberg-Bord et al., 2016; Murley and Nunnari, 2016). Studies in multiple organisms have demonstrated the physiological importance of organelle tethers in controlling metabolism, intracellular signaling, pathogen defense, and organelle inheritance (Helle et al., 2013; Prinz, 2014; Schrader et al., 2015; Eisenberg-Bord et al., 2016). Furthermore, it has been shown that organelle tethers can be dynamically regulated in response to changes in the cellular milieu, including metabolites and ions (Nhek et al., 2010; Hönscher et al., 2014; Kumagai et al., 2014). However, whether and how these structures are subject to developmental regulation to meet the demands of differentiation into new cell types is not clear.

A key cellular differentiation program in budding yeast is gametogenesis, which includes segregation of chromosomes by meiosis and the production of specialized gamete cells called spores. Various organelles, including mitochondria, undergo extensive remodeling during this process (Stevens, 1981; Miyakawa et al., 1984; Neiman, 1998; Fuchs and Loidl, 2004; Gorsich and Shaw, 2004; Suda et al., 2007; Tsai et al., 2014). Mitochondrial

[1]Department of Molecular and Cell Biology, University of California, Berkeley, Berkeley, CA; [2]Department of Genetics and Development, Columbia University Medical Center, New York, NY.

Correspondence to Elçin Ünal: elcin@berkeley.edu.

distribution changes dramatically during the meiotic divisions, when mitochondria lose their plasma membrane association, instead localizing near the gamete nuclei (Stevens, 1981; Miyakawa et al., 1984; Gorsich and Shaw, 2004). Subsequently, ~50% of the mitochondria from the progenitor cell is inherited by the gametes (Brewer and Fangman, 1980), and the remaining pool is eliminated (Eastwood et al., 2012; Eastwood and Meneghini, 2015). Although little is understood about the mechanisms responsible for mitochondrial reorganization and inheritance during meiosis, many other aspects of this developmental program, including transcriptional and cell cycle control, have been worked out in great detail in this organism (Marston and Amon, 2004; Neiman, 2011; van Werven and Amon, 2011; Winter, 2012). To what extent the previously identified meiotic regulators control mitochondrial dynamics and segregation has been unexplored.

In this study, we elucidated how mitochondrial reorganization is coordinated with meiotic development. We observed that mitochondria abruptly detach from the plasma membrane at the onset of anaphase II. To identify the mechanism responsible for regulating mitochondrial detachment, we examined a series of meiotic mutants with defects in meiotic progression. To our surprise, central meiotic regulators, such as the cyclin-dependent kinase CDK1/Cdc28 and the anaphase-promoting complex, were entirely dispensable for mitochondrial detachment. Instead, we found that the transcription factor Ndt80 and the meiosis-specific kinase Ime2 dictate the timing of mitochondrial detachment. Ndt80 controls mitochondrial detachment by inducing the expression of Ime2 and promoting its kinase activity (this study; Benjamin et al., 2003; Berchowitz et al., 2013). Ime2 phosphorylates both subunits of the MECA complex in vitro. Furthermore, Num1 undergoes Ime2-dependent phosphorylation in vivo. Finally, we show that Ime2 promotes MECA proteolysis, and this timely destruction of MECA drives mitochondrial detachment. Our results indicate that organelle tethering can be developmentally regulated to facilitate organelle remodeling, a feature of many cellular differentiation programs.

Results

Mitochondria detach from the plasma membrane in meiosis

To characterize the morphology and dynamic behavior of mitochondria during meiotic differentiation, we used time-lapse microscopy to monitor cells that simultaneously expressed fluorescent markers of mitochondria (Cit1-GFP) and the nucleus (Htb1-mCherry). Before the nuclear divisions, the mitochondrial network retained its characteristic morphology, existing as an interconnected tubular structure anchored to the cell cortex. Consistent with previous studies (Stevens, 1981; Miyakawa et al., 1984; Gorsich and Shaw, 2004), we found that mitochondria dissociated from the cell cortex during meiosis II (Fig. 1 A and Video 1). We term this phenomenon "mitochondrial detachment." Our data indicate that mitochondrial detachment occurs coincident with anaphase II. At the time of mitochondrial detachment, 68% of cells had begun anaphase II (Fig. 1 A). By 10 min after mitochondrial detachment, 90% of cells had initiated anaphase II.

To further determine the timing of mitochondrial detachment, we used two additional staging markers. The first marker,

GFP-Spo20[51–91], is an indicator of plasma membrane biogenesis that takes place as part of gamete maturation (Nakanishi et al., 2004; Neiman, 2011). Concomitant with the meiosis I to meiosis II transition, this process, termed prospore membrane formation, begins with fusion of vesicles at the yeast centrosomes, known as spindle pole bodies. As judged by changes in GFP-Spo20[51–91] localization, mitochondrial detachment occurred after membrane nucleation, but before the closure of the newly formed plasma membranes (Fig. 1 B and Video 2).

The second marker, Spc42-GFP, is a component of the spindle pole body. The distance between the duplicated spindle pole bodies is a reliable metric to determine the timing of metaphase to anaphase transition, because the spindle length increases approximately twofold during this period (Palmer et al., 1989; Kahana et al., 1995; Yeh et al., 1995). We measured when mitochondrial detachment took place with respect to changes in spindle length in cells carrying Spc42-GFP and Cit1-mCardinal. This analysis revealed that mitochondrial detachment occurred at the beginning of anaphase II (Fig. 1 C and Video 3). Hence, the timing of mitochondrial detachment is precise and occurs with stereotyped timing relative to other well-defined meiotic events.

Many canonical cell cycle regulators are dispensable for mitochondrial detachment

Because mitochondrial detachment occurred simultaneously with anaphase II onset, we reasoned that cell cycle regulators with characterized meiotic functions might jointly control the meiotic divisions and mitochondrial detachment. Because the initial steps of spore formation occur during meiosis II, active coupling of chromosome and organelle segregation could ensure gamete fitness. We monitored mitochondrial detachment and meiotic progression in strains carrying deletion or conditional alleles of genes encoding key cell cycle regulators (Fig. 2 A). We also noted that before meiotic entry, all of the mutants examined showed mitochondrial morphology indistinguishable from wild type, indicating that these alleles did not constitutively alter mitochondrial organization (Fig. 2, B–H). 8 h after induction of meiosis, the vast majority of wild-type cells contained four distinct nuclei that had not yet assembled into spores. In these cells, mitochondria invariably detached from the cortex and instead localized near the four postmeiotic nuclei (Fig. 2 B).

Among the cell cycle regulators that we analyzed, the polo kinase Cdc5, the anaphase-promoting complex activator Cdc20, and the cyclin-dependent kinase CDK1/Cdc28 are all essential for cell viability. To avoid perturbing the mitotic functions of these genes, we depleted CDC5 and CDC20 only from meiotic cells by replacing their promoters with the mitosis-specific CLB2 promoter (Lee and Amon, 2003). To down-regulate CDC28, we used a chemical inhibitor–sensitive allele, cdc28-as1 (Bishop et al., 2000). It has been reported that each mutant perturbs meiotic chromosome segregation: cdc5 and cdc20 mutants are defective in exiting metaphase I (Lee and Amon, 2003), whereas inactivation of cdc28-as1 in prophase I with 1-NM-PP1 inhibits meiosis I spindle assembly entirely (Benjamin et al., 2003). In each condition, the expected nuclear division defect was observed. However, mitochondrial detachment was unaffected. Mitochondria not only detached from the plasma membrane but
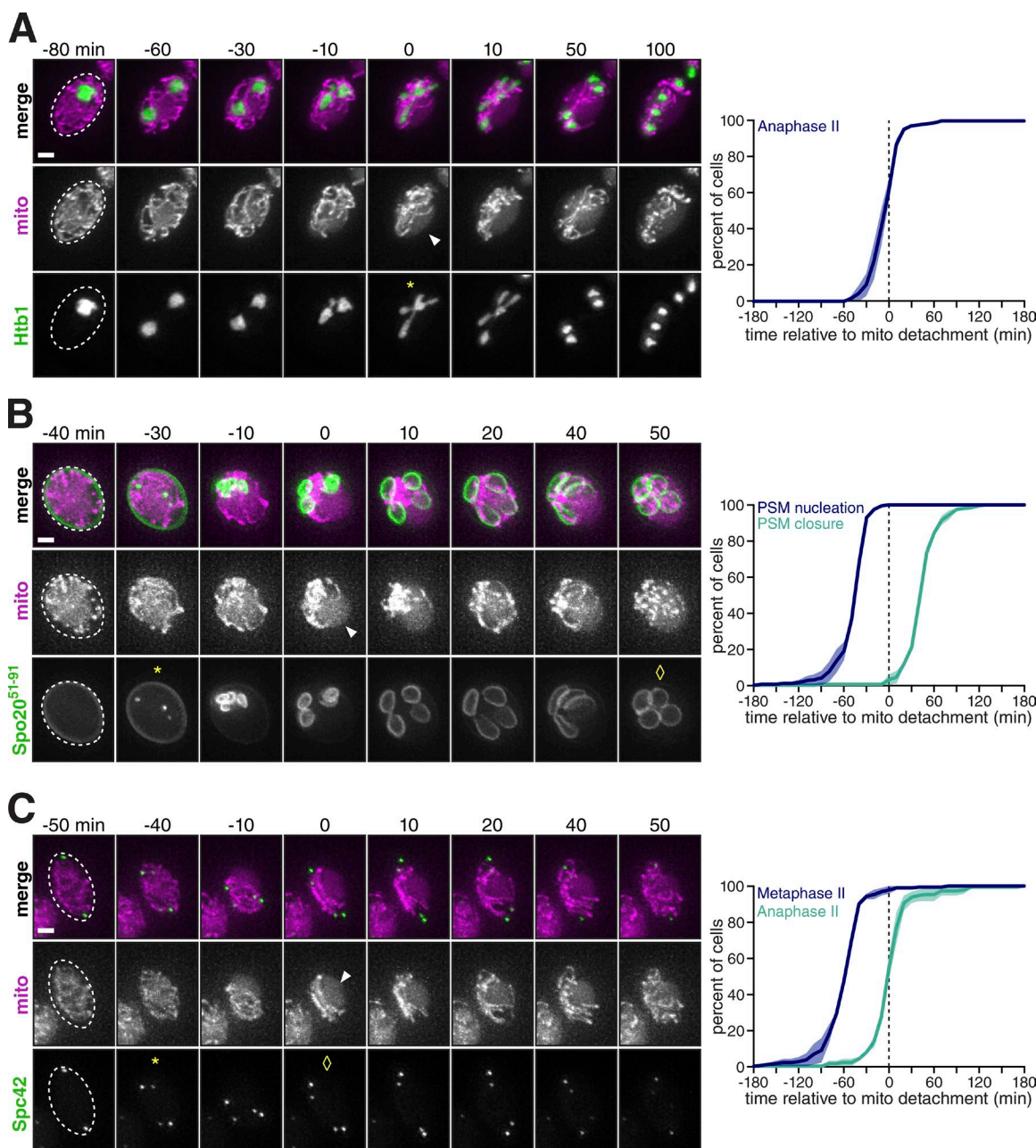
Figure 1. Mitochondria detach from the cell cortex during meiosis II. Video montages and quantifications of cells expressing Cit1-GFP or Cit1-mCardinal to label mitochondria (mito), as well as a meiotic staging marker, imaged every 10 min. Mitochondrial detachment is defined as the abrupt coalescence of mitochondria, showing restricted rather than uniform localization around the cell cortex (arrowhead). Dashed lines: cell boundaries. To determine the relative staging compared with markers of meiotic progression (below), mitochondrial detachment is defined to occur at 0 min. Plots show the mean ± range (shaded region) of two independent experiments ($n \geq 90$ cells counted per experiment per marker). **(A)** Mitochondrial detachment relative to the onset of the meiosis II nuclear division (anaphase II), marked by Htb1-mCherry (UB10257). Anaphase II is defined as the first appearance of a four-lobed nuclear morphology (*). **(B)** Mitochondrial detachment relative to prospore membrane nucleation and closure, marked by the GFP-Spo20[51–91] prospore membrane marker (UB13131). Prospore membrane nucleation is defined as the first appearance of Spo20[51–91] puncta (*) and closure as the rounding up of fully elongated prospore membranes (◊). **(C)** Mitochondrial detachment relative to metaphase II and anaphase II, marked by Spc42-GFP (UB13129). Metaphase II is defined as the first appearance of two pairs of separated Spc42-GFP dots (*). Anaphase II is defined as the first appearance of concerted movement separating the sister spindle pole bodies in each pair (◊). Scale bars, 2 µm.

also adopted their perinuclear localization, similar to wild-type cells (Fig. 2, C–E).

In addition to testing essential cell cycle regulators, we also assessed the role of nonessential regulators with defined meiotic functions. The Cdc14 Early Anaphase Release (FEAR) network controls the release of the Cdc28 antagonist phosphatase Cdc14 (Stegmeier et al., 2002; Yoshida et al., 2002). FEAR network signaling is absent in *spo12Δ* cells, which results in aberrant meiosis I spindle disassembly, culminating in the formation of binucleate postmeiotic cells instead of tetranucleate (Klapholz and
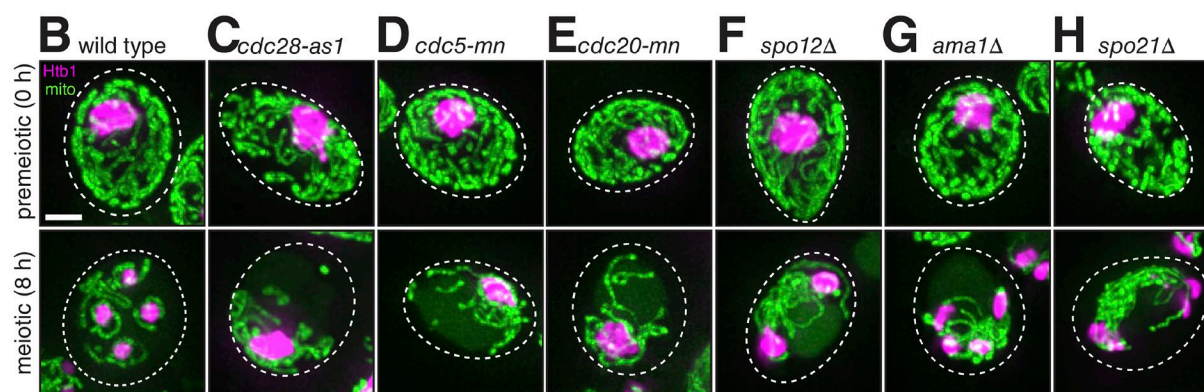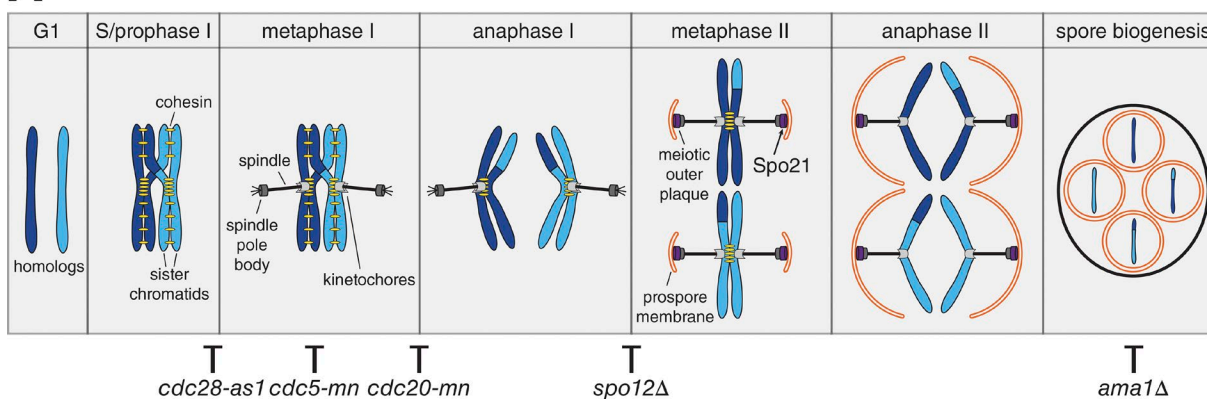
Figure 2. **Mitochondrial detachment is uncoupled from the meiotic divisions and spore development. (A)** Schematic of meiotic chromosome segregation and spore development. Meiotic regulators and spore development genes are labeled at key stages for their functions, where disruption of their function perturbs meiotic progression. **(B–H)** Maximum-intensity projections of fixed wild-type and mutant cells at 0 h (top) and 8 h (bottom) in SPO. Mitochondria (mito), mitoGFP or Cit1-GFP; nuclei, Htb1-mCherry. Dashed lines: cell boundaries. (B) Wild type (UB7155). (C) *cdc28-as1* synchronized by *pGAL-NDT80 GAL4.ER* (UB9494), with 1 µM 1-NM-PP1 and 1 µM β-estradiol added simultaneously at 5 h. (D) *cdc5-mn*, which is *pCLB2-CDC5* (UB7278). (E) *cdc20-mn*, which is *pCLB2-CDC20* (UB7343). (F) *spo12Δ* (UB7345). (G) *ama1Δ* (UB7533). (H) *spo21Δ* synchronized by *pGAL-NDT80 GAL4.ER* (UB9239). Scale bar, 2 µm.

Esposito, 1980; Marston et al., 2003; Kamieniecki et al., 2005). In *spo12Δ* cells, mitochondrial detachment was normal (Fig. 2 F). Mitochondrial detachment was also unaffected in *ama1Δ* cells (Fig. 2 G), which lack a meiosis-specific anaphase-promoting complex activator necessary for spore biogenesis (Cooper et al., 2000; Diamond et al., 2009).

Finally, we sought to address the possibility that prospore membrane formation is necessary for mitochondrial detachment, such as through sequestration of mitochondria into spores, because close proximity between mitochondria and prospore membrane has been observed (Suda et al., 2007). Synthesis of the prospore membrane requires assembly of a meiosis-specific structure on the cytoplasmic face of the spindle pole body, called the meiotic outer plaque (Knop and Strasser, 2000). In the absence of Spo21 (also known as Mpc70), a meiotic outer plaque component, other subunits fail to localize to the meiotic outer plaque, and therefore prospore membrane formation is completely disrupted (Knop and Strasser, 2000). We found that in *spo21Δ* cells, mitochondrial detachment was entirely unimpeded (Fig. 2 H). From these analyses, we conclude that much of the regulatory scheme that defines meiotic chromosome segregation and cellular differentiation is dispensable for mitochondrial de-

tachment and that other factors must be involved in regulating when and how mitochondria dissociate from the cell cortex.

The meiosis-specific transcription factor Ndt80 is required for mitochondrial detachment

We noted that in wild-type cells, mitochondrial morphology was indistinguishable at meiotic entry and prophase I, with mitochondrial detachment occurring abruptly during the second meiotic division. The master regulator controlling the transition to the meiotic divisions is the transcription factor Ndt80 (Xu et al., 1995; Chu and Herskowitz, 1998). Transcription of *NDT80* mRNA occurs during prophase I, but the ability of Ndt80 protein to localize to the nucleus is restricted by the pachytene checkpoint, which monitors the completion of double-strand break repair requisite for successful chromosome segregation (Chu and Herskowitz, 1998; Hepworth et al., 1998; Tung et al., 2000; Wang et al., 2011). In the absence of *NDT80*, cells exhibit a prolonged arrest during the pachytene stage of prophase I, failing to undergo meiotic divisions and subsequent gamete maturation (Xu et al., 1995).

To determine whether *NDT80* is required for mitochondrial detachment, we examined mitochondrial morphology in a

pGAL-NDT80 strain (Benjamin et al., 2003; Carlile and Amon, 2008). The *pGAL-NDT80* allele allows controlled induction of *NDT80* transcription by a β-estradiol activatable Gal4 fusion to the estrogen receptor protein (Gal4.ER; Benjamin et al., 2003; Carlile and Amon, 2008). In this background, typically >80% of cells perform the meiotic divisions. When we released cells from a 5-h Ndt80 block by addition of β-estradiol, mitochondrial detachment occurred normally (Fig. 3 A, +Ndt80). However, when the inducer was withheld, mitochondria remained persistently localized to the cell cortex (Fig. 3 A, –Ndt80), indicating that *NDT80* expression is necessary for mitochondrial detachment. *pGAL-NDT80* cells monitored by time-lapse microscopy showed identical behavior (Fig. S1 A and Videos 4 and 5). These experiments also confirmed that mitochondrial detachment is developmentally regulated and not an indirect outcome of prolonged nutritional deprivation. We conclude that Ndt80, a key regulator of meiotic events, is required for mitochondrial detachment.

Ime2 kinase is required for mitochondrial detachment

Ndt80 directly regulates the expression of ~200 genes (Chu and Herskowitz, 1998; Cheng et al., 2018). Among them, a particularly compelling candidate is the meiosis-specific kinase Ime2 (Smith and Mitchell, 1989; Yoshida et al., 1990; Kominami et al., 1993; Foiani et al., 1996; Nocedal et al., 2017). Ime2 belongs to a family of serine/threonine protein kinases displaying sequence similarities to both cyclin-dependent kinases and mitogen-activated protein kinases (Irniger, 2011). Although originally characterized as an early gene required for premeiotic S phase (Dirick et al., 1998), Ime2 kinase activity is significantly elevated during meiosis II (Benjamin et al., 2003; Berchowitz et al., 2013). It has been shown that Ndt80 is also necessary for the increase in Ime2 activity during meiosis II, independent of its role in regulating *IME2* expression (Benjamin et al., 2003; Berchowitz et al., 2013).

To determine whether Ime2 is necessary for mitochondrial detachment, we used a conditional allele, *ime2-as1*, that can be selectively inhibited by the drug 1-NA-PP1 (Benjamin et al., 2003). By controlling the timing of inhibitor treatment, we could bypass the requirement for Ime2 in premeiotic S phase. In cells arrested in prophase I by *pGAL-NDT80*, simultaneous addition of β-estradiol and 1-NA-PP1 resulted in retention of mitochondria at the cortex, even though cells performed meiosis I, as previously reported (Benjamin et al., 2003; Fig. 3 B). Mitochondrial detachment was normal in *IME2* wild-type cells that were identically treated, ruling out nonspecific effects of the drug treatment (Fig. 3 B). We obtained identical results by time-lapse microscopy (Fig. S1 B and Videos 6 and 7). These findings show that *IME2* function is necessary for mitochondrial detachment.

Ime2 regulates mitochondrial detachment independent of its role in Ndt80 activation

Our experiments thus far indicate that Ndt80, a transcription factor, and Ime2, a kinase, are involved in mitochondrial detachment. Previous studies found that Ndt80 is required for the elevated activity of Ime2 during the meiotic divisions (Benjamin et al., 2003; Berchowitz et al., 2013), and conversely, Ime2 is required for the accumulation of Ndt80 and its full activation

via phosphorylation (Sopko et al., 2002; Benjamin et al., 2003). Consequently, it was unclear whether the contribution of Ndt80 to the mitochondrial detachment phenotype was primarily by induction of Ime2, or the reverse model where the contribution of Ime2 is through enhancing Ndt80 activity. To distinguish between these possibilities, we induced *pGAL-NDT80* at 5 h but varied the timing of Ime2-as1 inhibition from 0.5 to 2.5 h after *NDT80* induction. We found that mitochondrial detachment was acutely sensitive to Ime2 inactivation. The frequency of mitochondrial detachment showed a graded response over 30-min intervals of drug-addition timing, with no drug-addition time point recapitulating the high frequency of mitochondrial detachment observed in wild-type cells (Fig. 3 C). As reference, by mRNA-seq (Brar et al., 2012), Ndt80 target genes are induced within ~1 h of *pGAL-NDT80* induction in wild-type cells. Addition of 1-NA-PP1 at 2.5 h after *NDT80* induction resulted in a mild effect on the meiotic divisions, yet mitochondrial detachment was still defective in a substantial fraction of the cells (Fig. 3, C and D). Although we cannot exclude the possibility that Ime2-as1 inactivation at later execution points might still compromise Ndt80 function, our results are most consistent with the model that the contribution of Ndt80 to mitochondrial detachment is principally through the regulation of Ime2 activity.

Next, we tested whether Ime2 could promote mitochondrial detachment in cells lacking a functional *NDT80* gene (*ndt80Δ*). For this, we used an *IME2* allele that has elevated activity throughout meiosis, *IME2-st* (Sia and Mitchell, 1995). Even though the absence of *NDT80* expression completely blocked meiotic progression, ~40% of the cells carrying the *IME2-st* allele displayed mitochondrial detachment (Fig. 3, E and F). The remainder had a typical, prophase I mitochondrial morphology. The basis of this heterogeneity is unclear at the moment, although a similar phenotype of incomplete penetrance has been observed in a previous study using the same allele (Berchowitz et al., 2013), potentially suggesting cell-to-cell variation in kinase activity. Nonetheless, these results demonstrate that Ime2 is sufficient to promote mitochondrial detachment and that the requirement of Ime2 for Ndt80 activation and meiotic divisions can be uncoupled from its role in mediating mitochondrial reorganization.

Finally, we sought to determine whether Ime2 is active in strains that are defective in meiotic progression but are capable of executing mitochondrial detachment. Although the elevated Ime2 kinase activity present during the meiotic divisions is known to require Ndt80 (Benjamin et al., 2003; Berchowitz et al., 2013), the precise requirements for Ime2 activation are unknown. We measured Ime2 kinase activity during meiosis in a subset of the mutants examined in Fig. 2. We found that, similar to wild-type Ndt80-induced meiotic cells, Ime2 kinase activity is elevated in *cdc5-mn*, *cdc28-as1*, and *cdc20-mn* cells after Ndt80 expression, despite the meiotic arrest phenotypes of these mutants (Fig. 4, A and B). In contrast, prophase-arrested (–Ndt80) cells do not activate Ime2, as evidenced by persistent low-level activity (Fig. 4 A). Our results are consistent with the interpretation that Ime2 is activated in a manner dependent on Ndt80 but independent of the cell cycle regulators examined, thereby explaining the uncoupling of mitochondrial detachment and meiotic progression shown in Fig. 2.
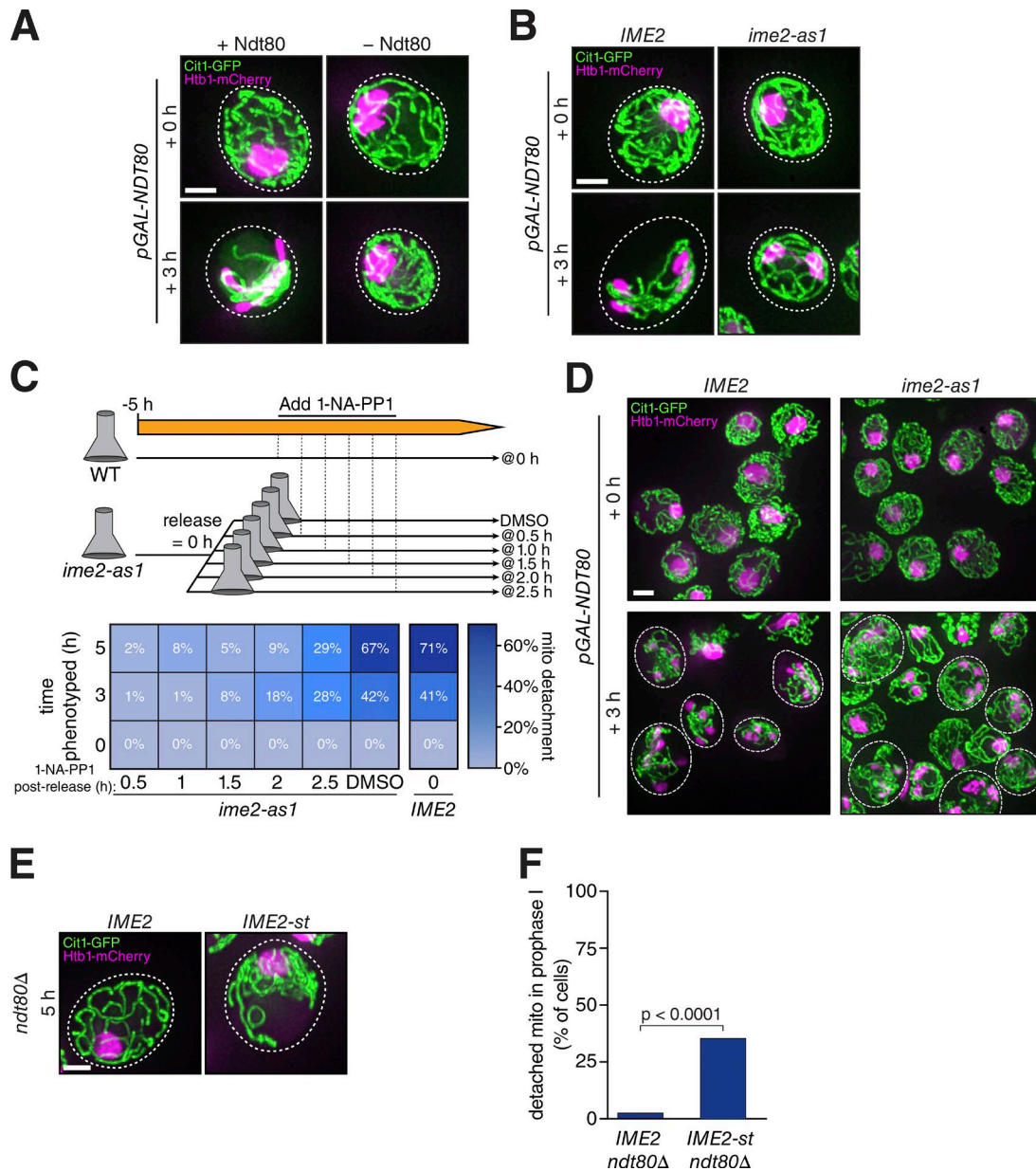
Figure 3. Ndt80 and Ime2 regulate mitochondrial detachment. (A) Maximum-intensity projections of fixed *pGAL-NDT80 GAL4.ER* cells (UB9496) with *NDT80* induced by addition of 1 µM β-estradiol (+Ndt80) or ethanol vehicle control (–Ndt80). Sporulation cultures were arrested for 5 h, then split and subjected to the indicated treatment. Cells were imaged 0 and 3 h after treatment. Mitochondria, Cit1-GFP; nuclei, Htb1-mCherry. Dashed lines: cell boundaries. **(B)** Maximum-intensity projections of fixed *pGAL-NDT80 GAL4.ER* cells containing wild-type *IME2* (UB9158) or *ime2-as1* (UB9844). Sporulation cultures were arrested for 5 h, then 1 µM β-estradiol and 20 µM 1-NA-PP1 were added simultaneously. Cells were imaged 0 and 3 h after treatment. Dashed lines: cell boundaries. **(C and D)** Execution point time course, with the timing of Ime2 inhibition varied relative to constant induction of *pGAL-NDT80*. (C) Top: Schematic of the execution point time course. Wild-type *pGAL-NDT80 GAL4.ER* (UB9158) and *pGAL-NDT80 GAL4.ER ime2-as1* (UB9844) were induced to sporulate and arrested for 5 h, then treated with 1 µM β-estradiol to induce *NDT80* (time = 0 h). Next, the *ime2-as1* culture was split and treated with 20 µM 1-NA-PP1 at the indicated time points relative to *NDT80* induction. DMSO served as the vehicle control and was added simultaneously with β-estradiol. The wild-type control was treated with 1-NA-PP1 and β-estradiol simultaneously. Bottom: Heat map showing the frequency of mitochondrial detachment at 0, 3, and 5 h after *NDT80* induction (i.e., the time of fixation) for each of the execution points (*n* = 2,200 total cells counted, with *n* ≥ 32 per panel in the heat map). (D) Maximum-intensity projections from wild-type control and the 2.5 h execution point. Dashed lines: cell boundaries for meiosis II cells only. **(E)** Maximum-intensity projections of prophase I arrested cells (*ndt80Δ*, 5 h in SPO) containing wild-type *IME2* (UB17328) or *IME2-st* (UB17330). Dashed lines: cell boundaries. **(F)** Quantification of mitochondrial morphology (percentage of cells with detached mitochondria) for the experiment in E (*n* = 100 per genotype). P < 0.0001, by Fisher's exact test. Scale bars, 2 µm.

The mitochondria-plasma membrane tether MECA is phosphorylated in an Ime2-dependent manner

How does Ime2 trigger mitochondrial detachment? A simple model would be that Ime2 inhibits the activity of a factor that normally connects mitochondria to the cell cortex. Because Ime2 is a protein kinase, such a factor could be an Ime2 substrate. A clear candidate was MECA (Cerveny et al., 2007; Klecker et al., 2013; Lackner et al., 2013). In mitotic cells, MECA tethers mitochondria to the plasma membrane by forming large assemblies at the contact sites between the two membranes (Cerveny et al.,
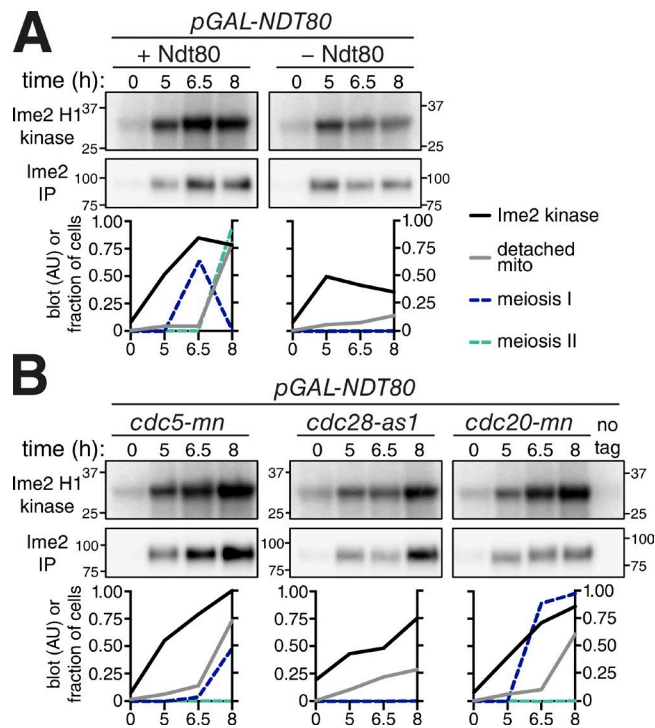
Figure 4. **Ime2 activation is uncoupled from meiotic progression.** Measurement of Ime2 kinase activity during meiosis in wild type and cell cycle mutants. Ime2-3V5 was immunoprecipitated from lysate collected at the indicated time points. On-bead Ime2-3V5 was incubated with histone H1 and γ-^{32}P ATP. Ime2 kinase activity toward histone H1 was determined by autoradiography, and Ime2-3V5 abundance in the reaction was determined by immunoblotting. Ime2 kinase activity is plotted with the background from a no-tag control (A15055) subtracted from each value. Values are scaled to the maximum background-subtracted value from the experiment. In addition, mitochondrial detachment frequency was scored using the Cit1-GFP mitochondrial marker and meiotic staging determined by tubulin immunofluorescence (n = 100 cells per time point per condition for each analysis). **(A)** pGAL-NDT80 GAL4.ER cells (UB10554) were induced to sporulate, then after 5 h treated with 1 µM β-estradiol (+Ndt80) or ethanol vehicle control (–Ndt80). **(B)** Sporulating pGAL-NDT80 GAL4.ER cdc5-mn (UB18612) and pGAL-NDT80 GAL4.ER cdc20-mn (UB18614) cells were treated with 1 µM β-estradiol at 5 h. pGAL-NDT80 GAL4.ER cdc28-as1 (UB18845) cells were simultaneously treated with 1 µM β-estradiol and 1 µM 1-NM-PP1 at 5 h.

2007; Klecker et al., 2013; Lackner et al., 2013). MECA has two known subunits, Num1 and Mdm36 (Lackner et al., 2013; Ping et al., 2016). Although Num1 can directly bind to lipids on both the outer mitochondrial membrane and plasma membrane, Mdm36 helps Num1 assemble into clusters at the membrane contact sites (Lackner et al., 2013; Ping et al., 2016). Interestingly, in the absence of MECA, mitochondria are constitutively detached from the plasma membrane in vegetative cells (Cerveny et al., 2007; Klecker et al., 2013; Lackner et al., 2013), which is highly reminiscent of the mitochondrial detachment that naturally occurs as part of meiotic differentiation.

To test whether Ime2 phosphorylates MECA, we first isolated recombinant Mdm36 and performed an in vitro kinase assay with constitutively active Ime2 (Ime2-st) purified from yeast. We found that Mdm36 was phosphorylated only in the presence of Ime2, suggesting that it is a direct substrate of the kinase (Fig. 5, A and B). To analyze Num1, we immunoprecipitated Num1-3V5

from vegetative cells and then performed a similar in vitro kinase assay. As with Mdm36, we observed Ime2-dependent phosphorylation of Num1 (Fig. 5 C). Together, these results demonstrate that Ime2 can phosphorylate both Num1 and Mdm36 in vitro.

We further found that Ime2 regulates MECA phosphorylation in vivo (Fig. 5 D). We isolated Num1 from prophase I–arrested cells (ndt80Δ) that expressed either wild-type Ime2 or the hyperactive Ime2-st and used label-free mass spectrometry (MS) to map phosphorylation sites. This approach led to the identification of four phosphorylated serine residues in Num1, one of which (S1094) was present only when Ime2 activity was high (Fig. 5 D). We used the same strategy to probe in vivo Mdm36 phosphorylation sites. However, we were unable to obtain sufficient amounts of the Mdm36-3V5 protein from meiotic cells, for even moderate peptide coverage, and no phosphorylation sites were detected (data not shown). We conclude that Num1, the major subunit of MECA, is phosphorylated in an Ime2-dependent manner during meiosis.

MECA undergoes dynamic changes in meiosis

To investigate a possible role of MECA in regulating mitochondrial dynamics during meiosis, we first examined the localization of Num1 and Mdm36. Similar to previous studies in vegetative cells (Cerveny et al., 2007; Tang et al., 2012; Klecker et al., 2013; Lackner et al., 2013; Ping et al., 2016; Kraft and Lackner, 2017), Num1 and Mdm36 formed prominent clusters at the cell cortex before meiosis II (Fig. 6 A); these foci represent contact sites between mitochondria and the plasma membrane. In contrast, meiosis II cells were devoid of Num1 and Mdm36 puncta. We further characterized MECA dynamics in meiosis by monitoring Num1-GFP localization in a strain carrying mitochondrially targeted blue fluorescent protein (mitoBFP) and Htb1-mCherry. In premeiotic and prophase I cells, we observed many bright Num1-GFP puncta, with mitochondria tethered at the plasma membrane (Fig. 6 B). In contrast, meiosis II cells were largely devoid of the puncta, and mitochondria were detached. The number of Num1 foci and total cellular fluorescence were significantly reduced in meiosis II cells compared with cells from earlier stages (Fig. 6, C and D). Furthermore, the disappearance of Num1 foci was dependent on Ndt80 expression (Fig. 6, B–D), but not on Cdc20 (Fig. S2A), consistent with our previous observations of mitochondrial behavior (Figs. 2 E, 3 A, and 4). These results strongly indicate that the timely detachment of mitochondria from the plasma membrane is driven by developmentally regulated changes in the MECA complex.

In a matched ribosome profiling and quantitative MS dataset generated from a yeast meiotic time course (Cheng et al., 2018), both Num1 and Mdm36 exhibit dynamic regulation during meiosis. Namely, as assessed by quantitative MS, the protein levels of Num1 and Mdm36 decrease as meiosis progresses, reaching their minima at 8 h (Fig. 6, E and F). We confirmed the decline in protein levels by immunoblotting with strains expressing epitope-tagged Num1-3V5 or Mdm36-3V5 from their endogenous loci (Fig. 6, G and H; and Fig. S3). In each case, protein decline occurred in an Ndt80-dependent manner (Fig. 6, G and H), suggesting that Num1 and Mdm36 protein levels are actively regulated.

The decline in Num1 and Mdm36 protein levels is not accompanied by a decrease in ribosome footprint density (Fig. 6, E and
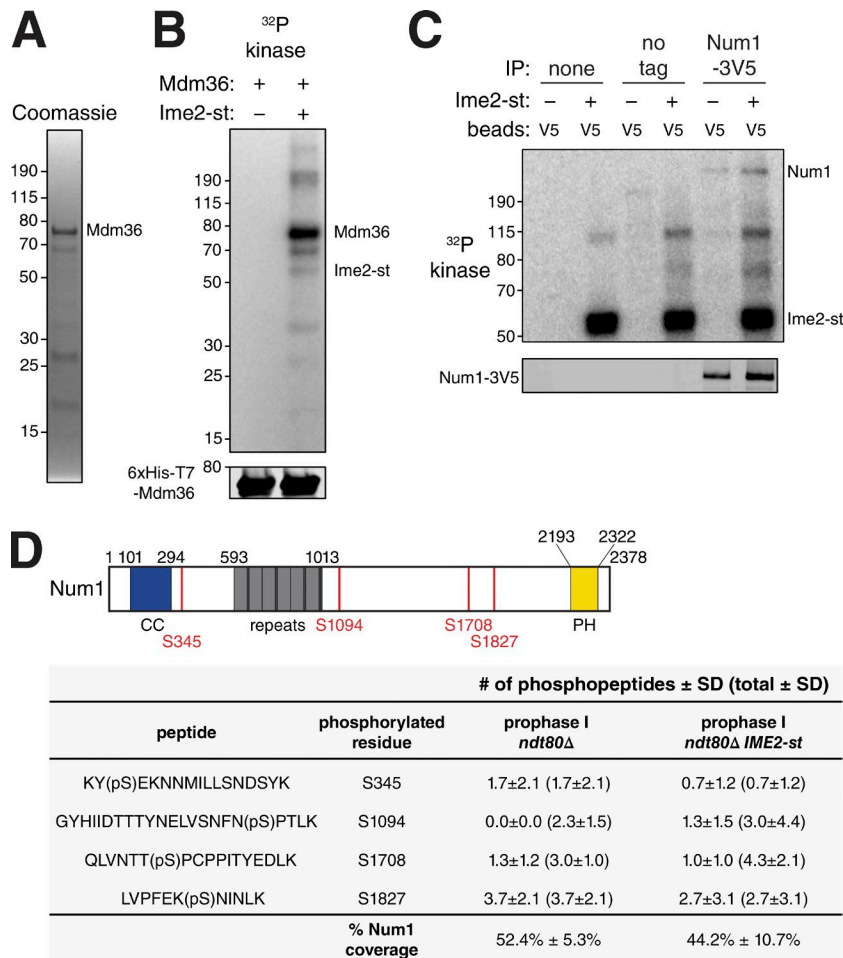
Sawyer et al.
Regulation of mitochondrial tethering in meiosis

Journal of Cell Biology
https://doi.org/10.1083/jcb.201807097

565

A

Coomassie

190
115
80 — Mdm36
70
50

30
25

15

B

^{32}P kinase

Mdm36: + +
Ime2-st: − +

190
115
80 — Mdm36
70 — Ime2-st
50

30
25

15

6xHis-T7 -Mdm36   80

C

IP: none | no tag | Num1 -3V5
Ime2-st: − + | − + | − +
beads: V5 V5 | V5 V5 | V5 V5

190   — Num1
^{32}P kinase   115
80
70
50   — Ime2-st

Num1-3V5

D

Num1   1 101 294   593   1013   2193 2322 / 2378

CC   S345   repeats   S1094   S1708 S1827   PH

peptide	phosphorylated residue	# of phosphopeptides ± SD (total ± SD)	
		prophase I *ndt80Δ*	prophase I *ndt80Δ IME2-st*
KY(pS)EKNNMILLSNDSYK	S345	1.7±2.1 (1.7±2.1)	0.7±1.2 (0.7±1.2)
GYHIIDTTTYNELVSNFN(pS)PTLK	S1094	0.0±0.0 (2.3±1.5)	1.3±1.5 (3.0±4.4)
QLVNTT(pS)PCPPITYEDLK	S1708	1.3±1.2 (3.0±1.0)	1.0±1.0 (4.3±2.1)
LVPFEK(pS)NINLK	S1827	3.7±2.1 (3.7±2.1)	2.7±3.1 (2.7±3.1)
% Num1 coverage		52.4% ± 5.3%	44.2% ± 10.7%

Figure 5. **Phosphorylation of Num1 and Mdm36 in vitro and in vivo. (A)** Coomassie-stained gel of 6xHis-T7-Mdm36 purified from *E. coli,* used in B. **(B)** In vitro kinase assays containing γ-^{32}P ATP, 1 μg recombinant Mdm36, and 3 pmol Ime2-st purified from yeast or no-kinase control. Reactions were incubated for 15 min at room temperature, then analyzed by SDS-PAGE and autoradiography. Before assembling the kinase assay, half of the input was reserved and analyzed by immunoblot. **(C)** In vitro kinase assay prepared as in B, but using on-bead substrate immunoprecipitated from vegetative cells using agarose beads conjugated with an anti-V5 antibody. Untagged lysate (no tag) was purified from wild type (UB15) and Num1-3V5 from strain UB12017. Beads never incubated with lysate (none) were also examined. Before assembling the kinase assay, half of the bead volume for each sample was reserved and bound protein was eluted and analyzed by immunoblot. Num1 runs above the highest (190-kD) ladder band. **(D)** Top: diagram of Num1 domain structure in the SK1 background and in vivo phosphorylation sites detected by MS (red lines and text). Black numbers refer to amino acid positions that define the domain boundaries. The Num1 amino acid sequence in SK1 differs from the S288C reference genome (Yue et al., 2017). Num1 (SK1) contains six copies of a 64-aa repeat, with some repeats separated by a spacer sequence (LEKEVEQ) and an overall length of 2,378 aa (271 kD). CC, coiled coil domain; PH, Pleckstrin homology domain. Bottom: Num1 phosphopeptides detected by LC-MS/MS from Num1-3V5 denaturing IP (see Materials and methods). pS, phosphoserine. The detected number of phosphopeptides and total peptides (phosphorylated and unmodified combined), as well as the overall sequence coverage of Num1 are shown for three biological replicates, is expressed as means ± SD. Num1-3V5 was isolated from *ndt80Δ* negative control cells (UB17332; prophase I *ndt80Δ*) and *ndt80Δ IME2-st* cells (UB16660; prophase I *ndt80Δ IME2-st*) after 5 h in SPO medium.

F), indicating that the abundance of Num1 and Mdm36 cannot be easily explained by regulation at the level of protein synthesis. Instead, we reasoned that Num1 and Mdm36 are actively degraded. To test whether the reduction in Num1 and Mdm36 protein levels requires the proteasome, a major conduit for protein degradation, we treated prophase I–arrested cells with the proteasome inhibitor MG-132 and simultaneously released them from the Ndt80 block. Upon MG-132 treatment, Num1 protein levels failed to decline to the extent seen in the control (Fig. 7 A); however, Mdm36 levels continued to decrease (Fig. 7 B). To assess proteasome dependence by an independent method, we used a hypomorphic allele of a 26S proteasome lid subunit, *rpn6-1* (Isono et al., 2005). Consistent with the MG-132 data, in *rpn6-1* cells, the protein levels of Num1, but not Mdm36, were stabilized throughout meiosis (Fig. S2, B and C), indicating proteasome dependence for Num1 degradation. To address the possibility that Mdm36 might instead be degraded by autophagy, we used the GFP-Mdm36 allele. Because GFP is relatively resistant to vacuolar degradation, autophagic degradation of the tagged protein leads to the accumulation of free GFP in the vacuole (Kanki and Klionsky, 2008). We observed free GFP by immunoblotting in late meiosis (Fig. 7, C and D), consistent with autophagy-dependent turnover of Mdm36. However, our data do not exclude the pos-

sibility of autophagy-independent processing of GFP-Mdm36. Altogether, these analyses reveal that programmed destruction of Num1 and Mdm36 causes the dissolution of MECA assemblies in meiosis II.

Ime2 induces mitochondrial detachment by promoting MECA degradation

What is the relationship between Ime2 and MECA in mediating mitochondrial detachment? We posited that Ime2 interferes with MECA function during meiosis II by promoting its destruction, thereby triggering mitochondrial detachment. To test this hypothesis, we first examined whether Ime2 regulates MECA stability by measuring Num1 and Mdm36 abundance in the *ime2-as1* mutant background. Treatment with 1-NA-PP1 at the time of *pGAL-NDT80* induction attenuated the degradation of Num1 and Mdm36 that was observed in wild-type cells (Fig. 8, A and B). Monitoring MECA assemblies in single cells yielded similar results (Fig. 8, C–F). Num1-GFP clusters persisted at later meiotic time points upon Ime2 inhibition (Fig. 8, C–E). Notably, the number of Num1 foci and overall Num1 intensity did not differ significantly between prophase I–arrested (+0 h) and Ime2-inhibited (+3 h) cells. In each case, mitochondria remained attached to the plasma membrane, presumably through the persistent contact
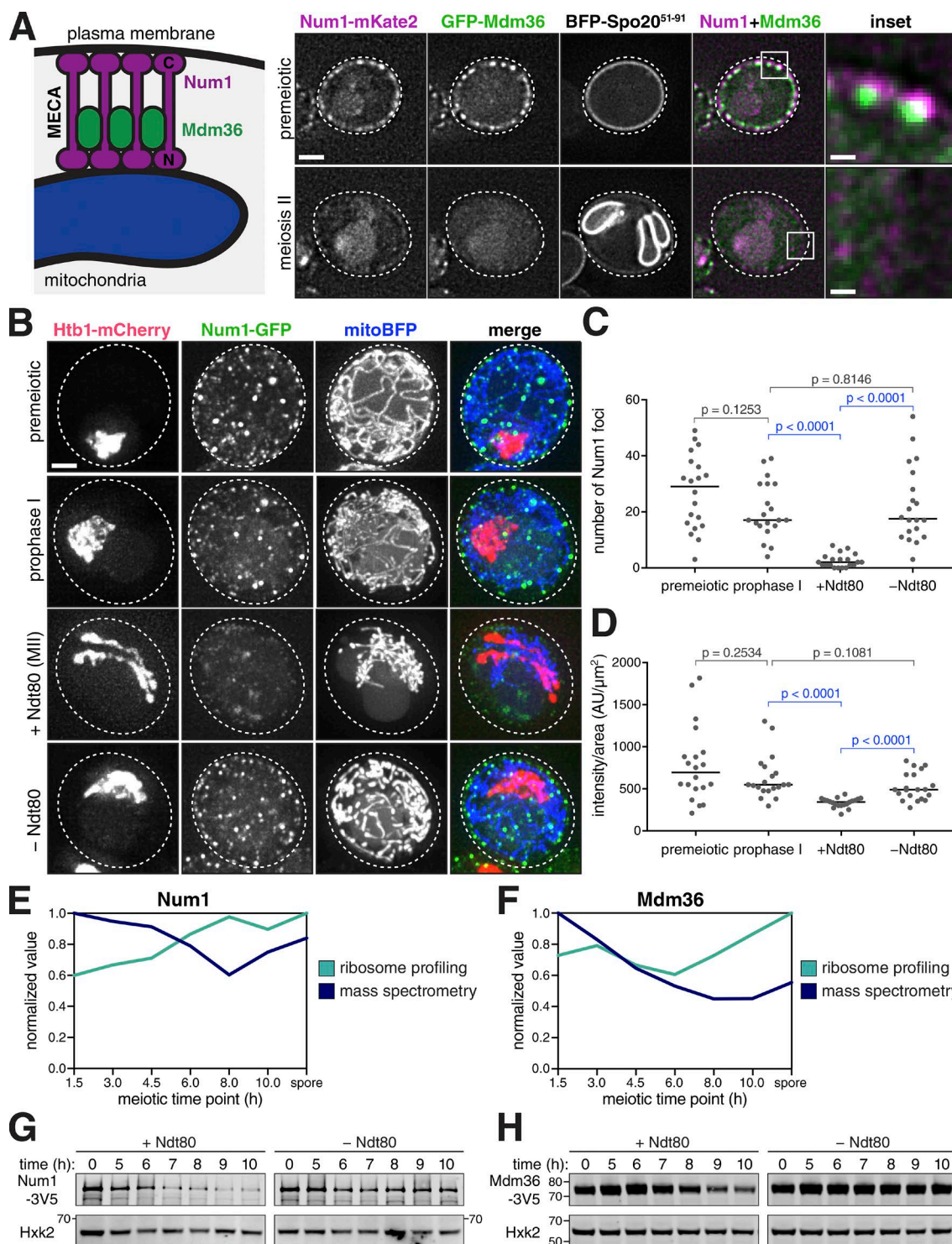
Sawyer et al.
Regulation of mitochondrial tethering in meiosis

Journal of Cell Biology   566
https://doi.org/10.1083/jcb.201807097

Figure 6.   **MECA is dynamically regulated in meiosis. (A)** Left: diagram of the mitochondria–plasma membrane contact site. MECA contains two known subunits, Num1 and Mdm36, and is responsible for tethering mitochondria to the plasma membrane. Right: localization of MECA subunits, Num1-mKate2 and GFP-Mdm36, in live premeiotic and meiosis II cells (UB16677). Single planes in the z-axis are shown. The meiotic stage was determined by the prospore membrane marker BFP-Spo20$^{51-91}$. **(B)** Maximum-intensity projections of live *pGAL-NDT80 GAL4.ER* cells (UB15124) showing MECA localization (Num1-GFP), mitochondrial localization (mitoBFP), and nuclei (Htb1-mCherry). Cells were imaged at time of transfer to SPO medium (premeiotic) and 5 h (prophase I). Then, at 5 h, the culture was split and treated with 1 μM β-estradiol (+Ndt80) or ethanol vehicle control (–Ndt80). Cells from the split cultures were imaged at 8 h. Dashed lines: cell boundaries. **(C and D)** Quantifications of the experiment in B. Analysis of the +Ndt80 sample was restricted to meiosis II stage cells (*n* = 20 cells per group). Medians are plotted as horizontal lines. The Mann–Whitney nonparametric test was used to test statistical significance. (C) Number of Num1-GFP foci per cell (see Materials and methods). (D) Whole-cell Num1-GFP fluorescence quantification from maximum-intensity projection, normalized to cell area. **(E and F)** Quantifications of Num1 and Mdm36 steady-state protein levels (MS) and synthesis (ribosome profiling) during meiosis from a published dataset (Cheng et al., 2018). **(G and H)** Immunoblots of MECA subunits in *pGAL-NDT80 GAL4.ER* strains. Strains were induced to sporulate for 5 h, then flasks were split and treated with 1 μM β-estradiol (+Ndt80) or ethanol vehicle control (–Ndt80). Hxk2 serves as a loading control. (G) Blot for Num1-3V5 (UB12402). Num1 runs above the highest (190-kD) ladder band. (H) Blot for Mdm36-3V5 (UB13851). Scale bars, 2 μm; inset panels, 400 nm.
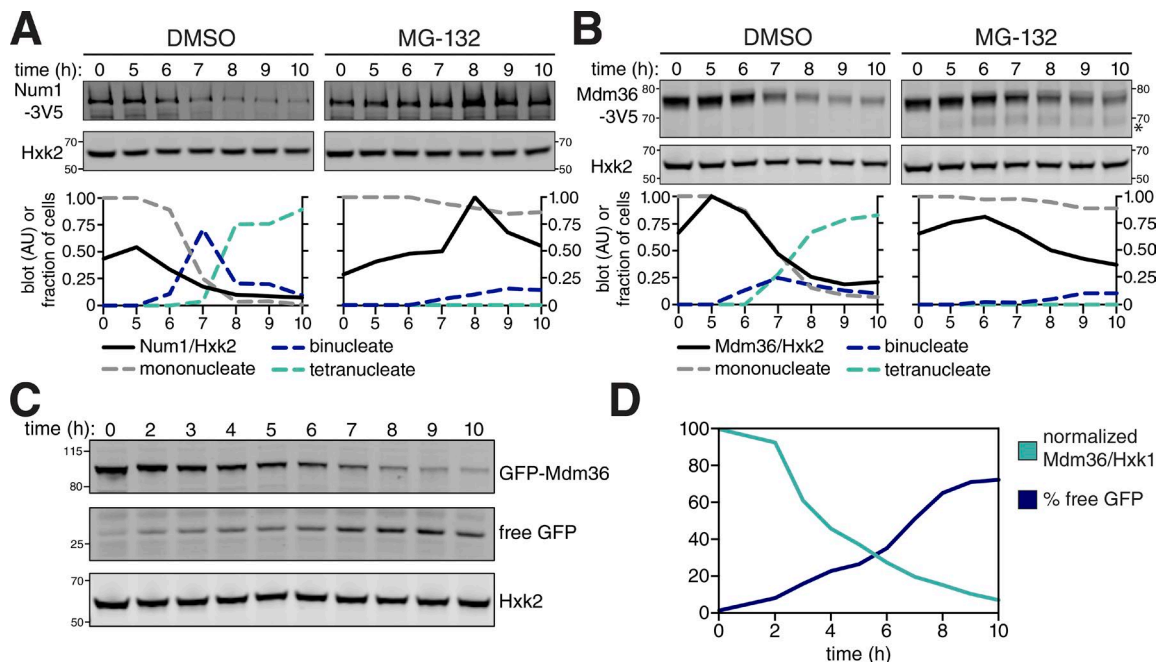
Figure 7. **MECA is destroyed by the proteasome and autophagy. (A and B)** Proteasome inhibition during meiosis by treatment with MG-132, compared with a DMSO vehicle control. Flasks were split at 5 h, with one half treated with 100 µM MG-132 and the other half with a DMSO vehicle control. Band intensity quantifications, normalized to the Hxk2 loading control, and time course staging by DAPI staining for each time point are shown below the immunoblots. (A) Immunoblot of Num1-3V5 in a *pGAL-NDT80 GAL4.ER* synchronous meiosis (UB13245), where 1 µM β-estradiol was added to the flasks at 5 h. Num1 runs above the highest (190-kD) ladder band. (B) Immunoblot of Mdm36-3V5 (UB16324). Asterisk: band of unknown identity. **(C)** Immunoblot autophagy assay of GFP-Mdm36 (UB16326). **(D)** Quantification of the blot in C. The total level of full-length protein (normalized Mdm36/Hxk2) was calculated as the intensity of the GFP-Mdm36 band divided by the Hxk2 loading control band. Percentages of the maximum value are plotted. The percentage free GFP value was calculated as the intensity of the free GFP band divided by the summed intensities of the free GFP and GFP-Mdm36 bands.

sites. Further, Num1 and Mdm36 remained colocalized after Ime2 inhibition (Fig. 8 F). The simplest interpretation of these data is that Ime2-dependent regulation leads to Num1 and Mdm36 degradation, which in turn causes MECA disassembly and mitochondrial detachment in anaphase II.

To further test the involvement of Ime2 in MECA destruction, we examined the impact of expressing the hyperactive Ime2-st kinase on MECA levels in prophase I–arrested cells. Both the number of Num1 foci and total cellular fluorescence decreased significantly upon *IME2-st* expression (Fig. 8, G–I). Our results indicate that elevated Ime2 activity in prophase I is sufficient to trigger premature Num1 degradation.

If Ime2 acts through MECA to promote mitochondrial detachment, then removal of MECA should restore normal mitochondrial dynamics to Ime2-inhibited cells. To test this hypothesis, we engineered a version of Num1 that can be degraded in an Ime2-independent manner (Fig. 9), using the auxin-inducible degron system (Nishimura et al., 2009). We found that forced destruction of Num1 rescued the mitochondrial detachment defect observed in *ime2-as1* cells (Fig. 9, B and C), highlighting Num1 as a key Ime2 target that is responsible for altering mitochondrial distribution during meiosis.

Discussion
In this study, we have shown that organelle morphogenesis during cellular differentiation can be accomplished by programmed removal of organelle tethers. MECA, which normally localizes to and maintains contact sites between mitochondria and the plasma membrane, is inactivated in meiosis II. As a consequence, mitochondria detach from the plasma membrane in a temporally coordinated manner. Mitochondrial detachment is regulated by the meiosis-specific kinase Ime2, which phosphorylates MECA and promotes its destruction (Fig. 10). Altogether, our study defines a key mechanism that coordinates mitochondrial dynamics with meiotic progression and demonstrates that organelle remodeling can be mediated by posttranslational regulation of organelle tethers.

Regulated destruction of an organelle tether acutely changes intracellular organization
In vegetative growth, MECA assembly in daughter cells is regulated during the cell cycle (Kraft and Lackner, 2017). Num1 exists in at least two distinct populations, one of which is independent of mitochondria and anchors cytoplasmic dynein at the bud tip (Omer et al., 2018). It is not clear, however, whether vegetative cells regulate the disassembly of MECA in any meaningful way. Once MECA is assembled, it is a very stable anchor: by FRAP, no appreciable recovery was observed over 20 min (Kraft and Lackner, 2017). Thus, it appears that MECA is a source of stability for an organelle that is otherwise highly dynamic in its architecture (Friedman and Nunnari, 2014; Mishra and Chan, 2014; Westermann, 2014).

During meiosis, MECA undergoes temporally coordinated disassembly. The timing of MECA destruction is determined by the level of Ime2 activity, which in turn is controlled by the mei-
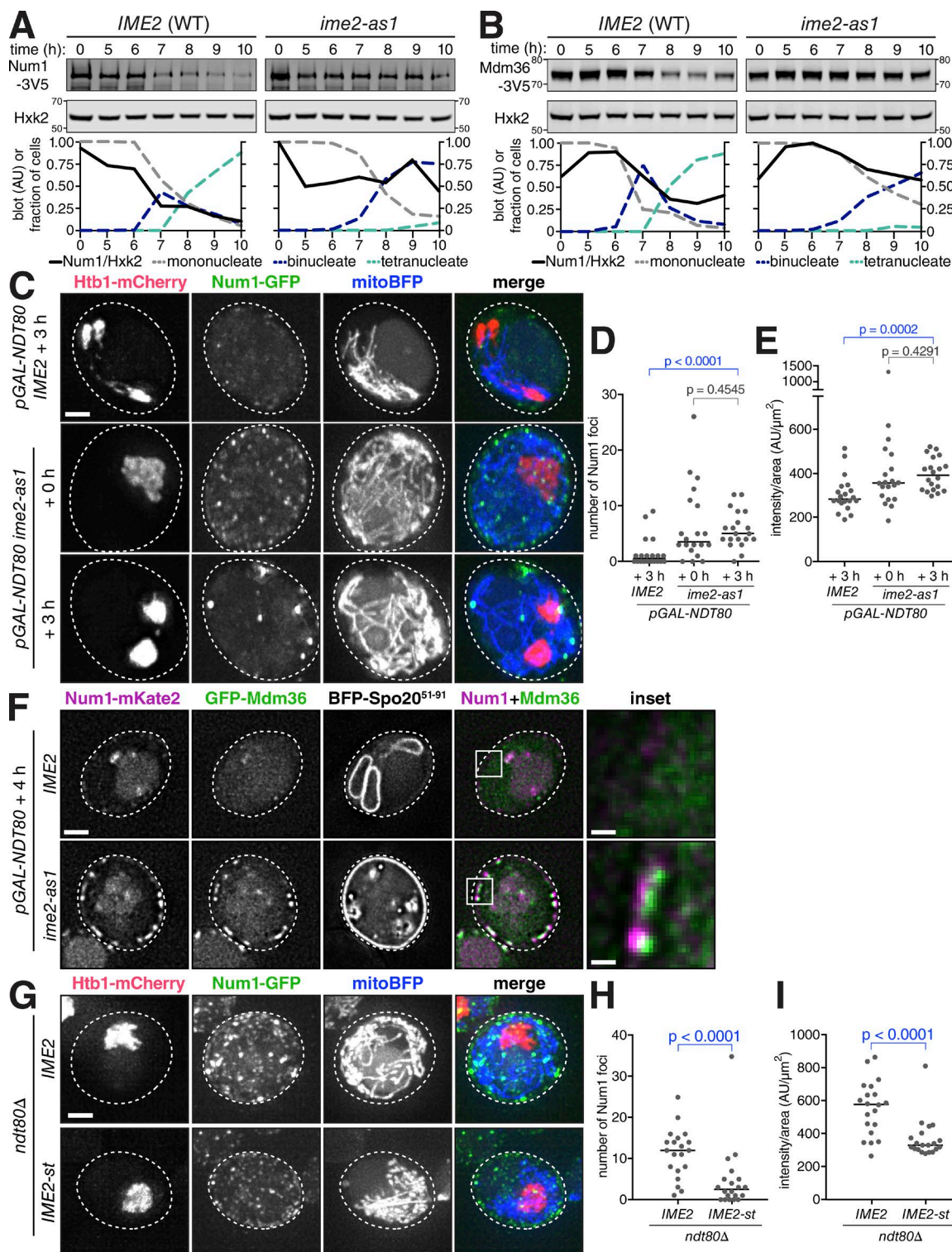
Figure 8. **Ime2 regulates MECA function in meiosis. (A and B)** Immunoblots of MECA subunits in *pGAL-NDT80 GAL4.ER.* Strains were induced to sporulate and were released 5 h later from prophase I arrest by the addition of 1 μM β-estradiol to induce *NDT80.* Simultaneously, 20 μM 1-NA-PP1 was added to inhibit *ime2-as1*, with wild-type *IME2* as the control. Band intensity quantifications normalized to the Hxk2 loading control and time course staging by DAPI staining for each time point are shown below the immunoblots. (A) Num1-3V5 immunoblot in wild type (UB12402) and *ime2-as1* (UB12403). Num1 runs above the highest (190-kD) ladder band. (B) Mdm36-3V5 immunoblot in wild type (UB13851) and *ime2-as1* (UB14546). **(C)** Maximum-intensity projections of live *pGAL-NDT80 GAL4.ER* cells containing wild-type *IME2* (UB15124) or *ime2-as1* (UB16047). Cells were induced to sporulate, then treated with 1 μM β-estradiol and 20 μM 1-NA-PP1 at 5 h. Images were acquired at the time of β-estradiol addition (0 h) or 3 h later. Dashed lines: cell boundaries. Mitochondria, mitoBFP. Nuclei, Htb1-mCherry. **(D and E)** Quantifications for the experiment in C. Analysis was restricted to cells that had entered the meiotic divisions (*n* = 20 cells per group). Medians are plotted as horizontal lines. The Mann–Whitney nonparametric test was used to test statistical significance. (D) Number of Num1-GFP foci per cell (see Materials and methods). (E) Whole-cell Num1-GFP fluorescence quantification from maximum-intensity projection, normalized to cell area.
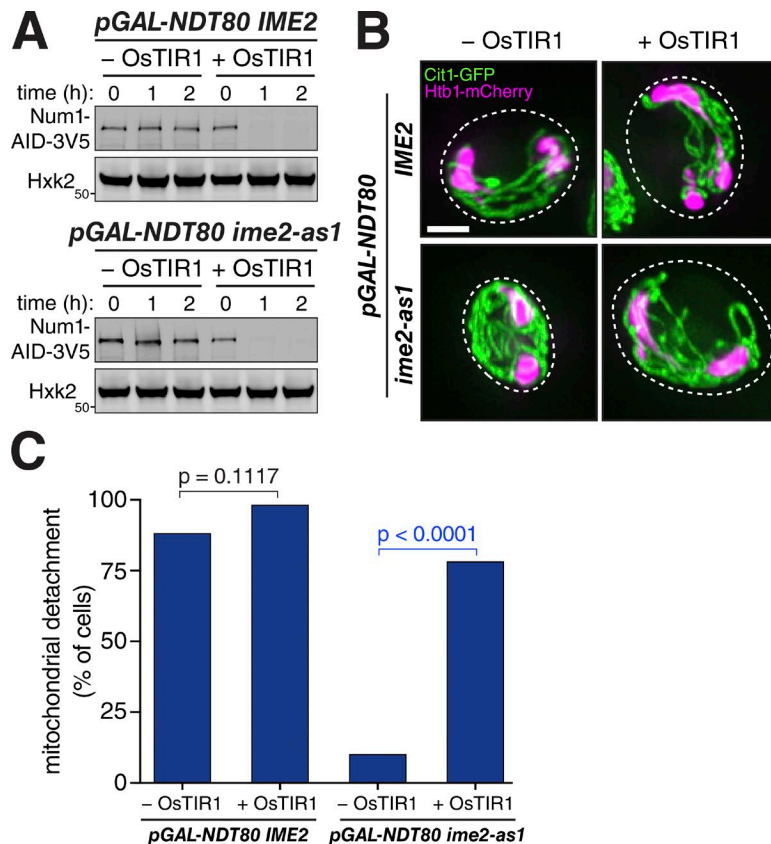
A

pGAL-NDT80 IME2

B

C

Figure 9. **Ime2 promotes mitochondrial detachment through MECA destabilization.** *pGAL-NDT80 GAL4.ER* cells without OsTIR1 (UB17552) and with *pCUP1-OsTIR1* (UB17548) as well as *pGAL-NDT80 GAL4.ER ime2-as1* cells without OsTIR1 (UB17554) and with *pCUP1-OsTIR1* (UB17550) were induced to sporulate. Then, 1 µM β-estradiol and 20 µM 1-NA-PP1 were added to the cultures at 5 h. At 6.5 h, 50 µM $CuSO_4$ and 500 µM 3-indoleacetic acid (auxin) were added. **(A)** Immunoblot showing Num1-AID-3V5 depletion. Hxk2, loading control. Time indicates hours after addition of auxin and $CuSO_4$ at 6.5 h, a time at which Num1 protein level was already reduced. By band quantification normalized to loading, Num1-AID-3V5 was 2.3× higher in level in *ime2-as1* (no OsTIR1) compared with the wild-type control (no OsTIR1). Num1-AID-3V5 runs above the highest (190-kD) ladder band. **(B)** Maximum-intensity projections of cells fixed 2 h after auxin and $CuSO_4$ addition. Mitochondria, Cit1-GFP; nuclei, Htb1-mCherry. **(C)** Quantification of the frequency of mitochondrial detachment among cells fixed 2 h after auxin and $CuSO_4$ addition. Analysis was restricted to cells that had entered the meiotic divisions (n = 50 cells per genotype). P = 0.1117, *IME2* −OsTIR1 vs. *IME2* +OsTIR1, by Fisher's exact test; P < 0.0001, *ime2-as1* −OsTIR1 vs. *ime2-as1* +OsTIR1. Scale bar, 2 µm.

otic transcription factor Ndt80. Our study demonstrates that an organelle tether can be developmentally regulated and reveals how this regulation could impact organelle remodeling. A similar principle might apply to other organelles and different developmental contexts.

In meiotic cells, the cortical ER detaches from the plasma membrane in a manner highly reminiscent of mitochondrial detachment (Suda et al., 2007). MECA destruction probably does not explain this behavior. Although ER has been observed in association with MECA by light microscopy and coimmunoprecipitation (Lackner et al., 2013), electron microscopy analysis did not reveal a significant association (Klecker et al., 2013). In addition, in neither case was it suggested that MECA acts to tether the ER to the plasma membrane. However, it has been recently shown that ER–plasma membrane anchoring proteins, Scs2/22, drive the assembly of a subset of MECA structures (Omer et al., 2018). Therefore, it is possible that loss of *SCS2* and/or *SCS22* function during meiosis could also contribute to MECA disassembly, although this perturbation alone is unlikely to explain the full extent of meiotic ER remodeling. ER–plasma membrane contacts are established by additional factors, including Tcb1/2/3 and Ist2,

which act redundantly with Scs2/22 (Manford et al., 2012). Based on the finding that removal of any one tether or class of tethers was insufficient for detachment of cortical ER from the plasma membrane, it would appear that meiotic cells have to target multiple tethers simultaneously to disrupt ER–plasma membrane contacts. Alternatively, changes intrinsic to the ER or plasma membrane, such as protein or lipid composition, may explain these phenomena. Interestingly, the plasma membrane pool of the lipid phosphatidylinositol 4,5-bisphosphate is depleted in late meiosis, instead accumulating on prospore membranes (Rudge et al., 2004).

Ime2 is a key regulator of mitochondrial dynamics in meiosis

Our studies reveal a distinct and unanticipated function for Ime2 during meiosis II: regulation of the mitochondria–plasma membrane tether MECA. Our data support a model in which Ime2 triggers MECA destruction by promoting the phosphorylation of its subunits, thereby causing acute changes in mitochondrial organization (Fig. 10). Several observations are consistent with this model. First, Ime2 phosphorylates both MECA subunits in vitro. Second, inactivation of Ime2 causes stabilization of

(F) Localization of Num1-mKate2 and GFP-Mdm36 in live *pGAL-NDT80 GAL4.ER* (UB18219) and *pGAL-NDT80 GAL4.ER ime2-as1* (UB18221) cells. After 5 h in SPO medium, the cultures were treated with 1 µM β-estradiol and 20 µM 1-NA-PP1. Images were acquired 4 h later. Single planes in the z-axis are shown. Entry into the meiotic divisions was staged by the prospore membrane marker BFP-Spo20[51–91]. Note that prospore membranes are misshapen in the *ime2* mutant. **(G)** Maximum-intensity projections of live wild-type *IME2 ndt80Δ* cells (UB16806) or *IME2-st ndt80Δ* cells (UB16808) arrested in prophase I for 5 h. Cells express the same cellular markers as in C. **(H and I)** Quantifications of the experiment in G (n = 20 cells per group). Medians are plotted as horizontal lines. The Mann–Whitney nonparametric test was used to test statistical significance. (H) Number of Num1-GFP foci per cell (see Materials and methods). (I) Whole-cell Num1-GFP fluorescence quantification from maximum-intensity projection, normalized to cell area. Scale bars, 2 µm; inset panels, 400 nm.
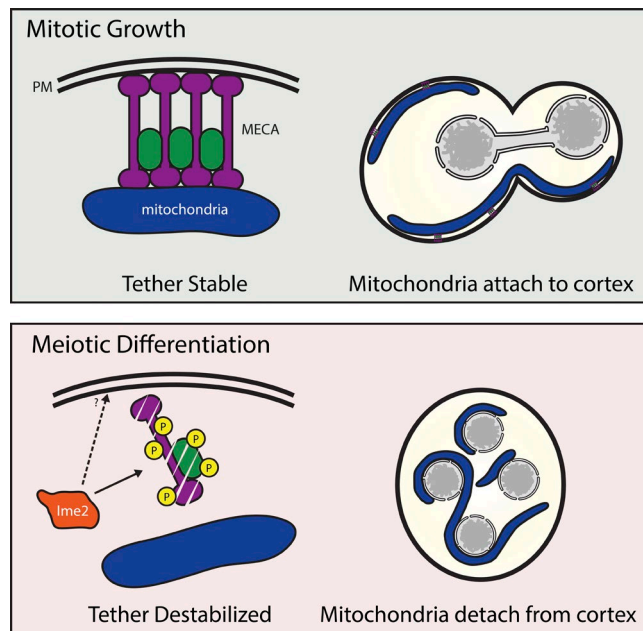
Figure 10. **Mitochondrial inheritance in mitosis and meiosis.** In mitosis, mitochondria remain associated with the cell cortex because of the mitochondria–plasma membrane anchoring activity of MECA. In meiosis, mitochondrial organization is remodeled: Mitochondria detach from the plasma membrane and are transmitted to spores. This meiosis-specific mitochondrial remodeling is caused by the inhibition of MECA by Ime2. As a result of Ime2-dependent phosphorylation, MECA is destroyed, and mitochondrial tethering is lost. PM, plasma membrane; P, phosphate.

MECA subunits, persistence of MECA clusters, and retention of contacts between mitochondria and the plasma membrane throughout meiosis. Third, expression of a hyperactive *IME2* allele in prophase I leads to Num1 phosphorylation and results in the premature disassembly of MECA and untimely mitochondrial detachment. Finally, degradation of Num1 by artificial means rescues the mitochondrial detachment defect that occurs in *IME2*-inactivated cells. Our data, however, do not rule out the possibility that Ime2 can also influence MECA in an indirect manner (Fig. 10), for instance through its effect on other, yet to be identified, MECA regulators.

Ime2-dependent destruction of MECA shares similarities with another critical meiotic event: clearance of the translational repressor Rim4. Rim4 assembles into amyloid-like aggregates, which are thought to sequester a group of mRNAs away from ribosomes by binding to their 5′ UTRs (Berchowitz et al., 2013, 2015; Carpenter et al., 2018). Degradation of Rim4 during meiosis II relieves the translational repression of its targets. Similar to MECA, high Ime2 kinase activity is both necessary and sufficient to disassemble Rim4 aggregates and promote their degradation (Berchowitz et al., 2013, 2015; Carpenter et al., 2018). Rim4 contains a total of 114 serine and threonine residues (S/Ts). Although the initial MS suggested the existence of a single Ime2-dependent phosphorylation site, subsequent work identified 39 additional phosphorylation sites. Clearance of Rim4 assemblies is governed by multisite phosphorylation, with at least 36 S/Ts necessary for its degradation. Importantly, a threshold amount of phosphory-

lation, rather than modification of critical residues, is necessary for Rim4 clearance (Carpenter et al., 2018). By comparison, Num1 contains 356 S/Ts. Thus far, MS identified four phosphorylated residues in Num1, one of which appears to be Ime2 dependent. However, this number is likely to be an underestimate, because the peptide coverage for Num1 was <60% in our immunoprecipitation (IP)-MS analysis. Moreover, unlike the Rim4 IP-MS, our experiments did not include a phosphopeptide enrichment step due to the low expression level of Num1. Adding further to the complexity is the observation that the second MECA subunit, Mdm36, also appears to be phosphorylated by Ime2. Therefore, MECA control by Ime2 is likely to be complex. More thorough analysis is needed to elucidate how phosphorylation affects MECA stability, mitochondrial organization, and inheritance.

Mitochondrial inheritance during gametogenesis

How does mitochondrial detachment lead to meiosis-specific inheritance of the organelle? In budding yeast, mitochondria exhibit four distinct behaviors during meiotic differentiation: (a) abrupt detachment from the mother cell plasma membrane, followed by (b) extensive contacts with the gamete nuclei, (c) limited inheritance, and (d) programmed elimination. Previous EM data suggested that only about half of the starting mitochondrial population is inherited by the four gametes (Brewer and Fangman, 1980). The remaining mitochondria are eliminated by mega-autophagy that commences at the end of gametogenesis (Eastwood et al., 2012; Eastwood and Meneghini, 2015). It will be interesting to determine whether the two populations of mitochondria—namely, the inherited and discarded—are different from one another and whether quality control pathways exist to selectively transmit healthier mitochondria to gametes (Neiman, 2011; Kraft and Lackner, 2018). Perhaps the ability of mitochondria to form direct contact sites with the nuclear envelope, evident in Fig. 2 and previous studies (Stevens, 1981; Suda et al., 2007), is part of this selection. Regardless, we propose that the contact sites between mitochondria and nuclear envelope ensure that the mitochondrial genome is inherited during yeast gametogenesis. We further posit that the regulated detachment of mitochondria from the progenitor cell plasma membrane in meiosis II is the first step toward mitochondrial segregation into gametes. Identifying the molecular nature of the mitochondria–nuclear contact sites and their regulation will enhance our understanding of mitochondrial inheritance during meiotic differentiation.

Gametogenesis-specific changes to mitochondrial architecture and inheritance are ubiquitous in metazoan germ cells. For example, primary oocytes of animals contain a unique structure known as the Balbiani body that assembles adjacent to the nucleus (Kloc et al., 2004). The Balbiani body houses a collection of organelles, including mitochondria and protein–RNA inclusions, and facilitates their segregation. In *Drosophila melanogaster* oogenesis, mitochondria are transported between cells, from nurse cells to the oocyte, via a polarized microtubule network that passes through ring canals (Cox and Spradling, 2003). Later, mitochondria are actively tethered to the actin cytoskeleton at the posterior of the oocyte, in proximity to the pole cells that give rise to the germline. Importantly, in the absence of tethering, mtDNA transmission is compromised

Sawyer et al.
Regulation of mitochondrial tethering in meiosis

Journal of Cell Biology   571
https://doi.org/10.1083/jcb.201807097

(Hurd et al., 2016). Although sperm contain mitochondria to meet metabolic demands, they do not transmit genetic information to the zygote. In *Drosophila*, mtDNA is actively destroyed during spermatogenesis (DeLuca and O'Farrell, 2012). In mice, sperm mitochondria are delivered to the zygote, but are depolarized, unable to fuse to maternal mitochondria, and are specifically eliminated by mitophagy (Rojansky et al., 2016). Clearly, mitochondria undergo a plethora of changes during metazoan gametogenesis, which share striking similarities to that observed in budding yeast gametogenesis: nuclear–mitochondrial interactions and programmed mitochondrial elimination. We speculate that the evolutionary conservation of meiotic differentiation between budding yeast and metazoans extends beyond homologous recombination and meiotic chromosome segregation.

Understanding the molecular basis of meiotic specializations to mitochondria is important, not only to enhance our understanding of the organelle's physiology, but also for its potential impact on human disease and health span. It is widely observed that mitochondrial function declines with age, yet gametogenesis, at least in budding yeast and *Caenorhabditis elegans*, eliminates age-induced cellular damage (Goudeau and Aguilaniu, 2010; Unal et al., 2011; Bohnert and Kenyon, 2017). Therefore, studying mitochondria in the context of gametogenesis could aid in the development of strategies to counteract mitochondrial dysfunction and disease.

Materials and methods

Yeast strains and plasmids

All yeast strains used in this study are derivatives of SK1 (Padmore et al., 1991), except for B114, and are described in Table S1. The Ndt80 block–release system and associated strains were described previously (Benjamin et al., 2003; Carlile and Amon, 2008) and contain *pGAL-NDT80* and *GAL4.ER* transgenes. The PP1 analogue sensitive kinase alleles *cdc28-as1* (F88G; Bishop et al., 2000) and *ime2-as1* (M146G; Benjamin et al., 2003) have been described. The *IME2-st* allele was described previously (Sia and Mitchell, 1995) and lacks the C-terminal 241 amino acids. Meiotic-null alleles generated by promoter replacement using *pCLB2* were described for *CDC5* and *CDC20* (Lee and Amon, 2003). The *rpn6-1* (*435Y) allele was described previously (Isono et al., 2005) as was the His3MX6-marked SK1 version of the strain (Carpenter et al., 2018). The untagged control strain, A15055, for the Ime2-3V5 IP experiment (Berchowitz et al., 2013), as well as the auxin-inducible degron system (Nishimura et al., 2009), were described previously. In this study, we used TIR1 from *Oryza sativa* under regulation of the copper-inducible promoter *pCUP1*. The *pCUP1-OsTIR1* construct was cloned into the *HIS3* single integration vector pNH603 (Youk and Lim, 2014), but modified to remove homology to the *DED1* locus (a gift from L. Chan, University of California, Berkeley, Berkeley, CA). The Num1-AID allele carried a C-terminal IAA7 degron followed by a 3V5 tag. The IAA7-3V5 tagging plasmid was a gift from L. Chan.

Yeast transformation was performed using the lithium acetate method. C-terminal tagging was performed using a PCR-mediated technique previously described (Longtine et al., 1998; Janke et al., 2004). As some C-terminally tagged alleles of *MDM36* are not functional, we verified functionality of *MDM36-3V5* using an established assay (Fig. S3; Lackner et al., 2013). We constructed a *LEU2*-selectable GFP(S65T) tagging plasmid by replacing the selectable marker in pFA6a-GFP(S65T)-His3MX6 with *Candida glabrata LEU2* (*cgLEU2*), amplified from pLC605 (a gift from L. Chan). The 3V5 tagging plasmid was a gift from V. Guacci (University of California, Berkeley, Berkeley, CA).

To visualize mitochondria, we used several different strategies. First, we C-terminally tagged *CIT1* with a fluorescent protein, as described (Higuchi-Sanabria et al., 2016), using GFP(S65T) or mCardinal (Chu et al., 2014). The mCardinal yeast tagging plasmid was a gift from R. Higuchi-Sanabria (University of California, Berkeley, Berkeley, CA). We also expressed the Su9 mitochondrial targeting sequence from *Neurospora crassa* fused to yeast-enhanced GFP (yEGFP) under regulation of a *pGPD1* promoter, expressed from a pNH603 single integration plasmid (Youk and Lim, 2014), but modified to remove homology to the *DED1* locus (a gift from L. Chan). Last, we expressed a mitoBFP construct from a pRS424 plasmid modified to carry a KanMX or NatMX marker instead of *TRP1* (termed pRS(2μ)-KanMX or -NatMX). The mitoBFP construct was described as pYES-TagBFP (Murley et al., 2013), and pRS424 was described previously (Christianson et al., 1992).

To visualize the prospore membrane, we fused amino acids 51–91 from Spo20 (Nakanishi et al., 2004) to the C terminus of link-yEGFP (Sheff and Thorn, 2004) or mTagBFP2, under regulation of the *ATG8* promoter (amplified from pRS306-2xyEGFP-ATG8; Graef et al., 2013), subcloned into the *LEU2* integrating plasmid pLC605 (a gift from L. Chan) or a pRS(2μ), drug-selectable plasmid (described in the previous paragraph).

To generate the *GFP-MDM36* strain, we used a Cas9-mediated genome editing strategy similar to a described method (Anand et al., 2017). Annealed oligonucleotides encoding the guide RNA (5'-GAACACTTACTACTATAGCA-3') were inserted into a centromeric plasmid carrying a *URA3* marker and *pPGK1-Cas9* (a gift from G. Schlissel, University of California, Berkeley, Berkeley, CA), generating pUB1395. Then, pUB1395 and a repair template were cotransformed into yeast, the plasmid was lost by streaking cells without selection, and the presence of the yEGFP tag was confirmed by PCR and sequencing.

To purify Mdm36 from *Escherichia coli*, we used an IPTG-inducible expression plasmid described previously as pET22b mod T7prom::H6-T7-Mdm36 (Ping et al., 2016) and provided by L. Lackner (Northwestern University, Evanston, IL). (See below for protein purification method.)

Sporulation

Unless indicated otherwise, cells were induced to sporulate by a traditional starvation synchronization method. At all steps, flasks were shaken at 275 rpm. First, cells were grown in YPD (1% yeast extract, 2% peptone, 2% glucose, 22.4 mg/l uracil, and 80 mg/l tryptophan) for ~24 h at room temperature to reach saturation ($OD_{600} \geq 10$). The YPD culture was used to inoculate BYTA medium (1% yeast extract, 2% bacto tryptone, 1% potassium acetate, and 50 mM potassium phthalate) to $OD_{600} = 0.25$ and grown for ~16 h at 30°C to reach $OD_{600} \geq 5$. Then, the cells were pelleted,

Sawyer et al.
Regulation of mitochondrial tethering in meiosis

Journal of Cell Biology
https://doi.org/10.1083/jcb.201807097

572

washed with sterile water, and resuspended to a density of OD_{600} = 1.85 in sporulation (SPO) medium (0.5% potassium acetate and 0.02% raffinose, pH 7). Cultures were shaken at 30°C for the duration of the experiment. In cases where selection for plasmids was necessary, G418 (Geneticin) or nourseothricin (clonNAT) was added to YPD and BYTA cultures at concentrations of 200 and 100 µg/ml, respectively.

In experiments using synchronization by the Ndt80 block–release system, cells carrying the *pGAL-NDT80* and *GAL4.ER* transgenes were induced to sporulate as described above. After 5 h in SPO medium, β-estradiol was added to a final concentration of 1 µM from a 5-mM stock (in ethanol) to induce *NDT80* expression.

Microscopy

All images were acquired with a DeltaVision Elite wide-field fluorescence microscope (GE Healthcare) and a PCO Edge sCMOS camera, operated by the associated softWoRx software. Time-lapse imaging experiments were performed in an environmental chamber heated to 30°C, with images acquired with a 60×/NA1.42 oil-immersion Plan Apochromat objective. Cells were maintained on concanavalin A–coated, glass-bottom 96-well plates (Corning). Every 10 min, a stack of 8 Z positions (1-µm step size) was acquired, with mCherry (32% intensity, 25-ms exposure) and FITC (10% intensity, 25-ms exposure) filter sets. All other imaging experiments were acquired at ambient temperature (~22°C) with a 100×/NA1.4 oil-immersion Plan Apochromat objective. All live cells were imaged in SPO medium. Where indicated, cells were fixed at room temperature for 15 min by adding formaldehyde (final concentration of 3.7%) directly to the culture medium. To halt fixation, cells were washed once with 100 mM potassium phosphate, pH 6.4, and stored in 100 mM potassium phosphate, pH 7.5, with 1.2 M sorbitol at 4°C. All fixed samples were imaged in 100 mM potassium phosphate, pH 7.5, with 1.2 M sorbitol. All images were deconvolved in softWoRx software (GE Healthcare) with a 3D iterative constrained deconvolution algorithm (enhanced ratio) with 15 iterations. Linear adjustments to brightness and contrast were made in Fiji (Schindelin et al., 2012).

Image quantification

Num1-GFP spot number and Num1-GFP fluorescence intensity were measured in Fiji. First, the mean background intensity was measured in a 155 × 155-pixel square containing no cells. This value was then subtracted from each pixel in the image. Next, cells were manually traced, and the Find Maxima function was run to identify spots (noise tolerance = 1,500) within the traced region. In addition, the total fluorescence intensity (IntDen) and area were measured for each cell.

Statistical analysis

All tests of statistical significance were nonparametric (Mann–Whitney test or Fisher's exact test) and performed in Prism (GraphPad Software). The results from all statistical tests are reported as two-tailed P values.

Time course staging by DAPI staining and tubulin immunofluorescence

Cells collected from meiotic culture at the desired time points were fixed in 3.7% formaldehyde overnight at 4°C. Then, cells were pelleted, washed once with 100 mM potassium phosphate, pH 6.4, and stored in 100 mM potassium phosphate, pH 7.5, with 1.2 M sorbitol at 4°C.

For DAPI staining, cells were mounted on poly-L-lysine–coated multiwell slides. Then, slides were submerged in −20°C methanol for 3 min followed by −20°C acetone for 10 s. After drying, the slide was filled with VectaShield Antifade Mounting Medium with DAPI (Vector Labs) and sealed with a coverslip.

For tubulin immunofluorescence, fixed cells were resuspended in 200 µl of 100 mM potassium phosphate, pH 7.5, with 1.2 M sorbitol, to which 20 µl of glusulase (Perkin-Elmer) and 6 µl of 10 mg/ml zymolyase 100T (MP Biomedicals) were added to obtain spheroplasts. Digestions were incubated at 30°C with rotation for 2–3 h. Completion of the digestion was monitored by sensitivity of a small aliquot of cells to lysis in the presence of 0.5% SDS. Spheroplasts were gently pelleted (900 g) and gently resuspended in 500 µl of 100 mM potassium phosphate, pH 7.5, with 1.2 M sorbitol as a wash step. Spheroplasts were then pelleted again and resuspended in 10–50 µl of 100 mM potassium phosphate, pH 7.5, with 1.2 M sorbitol. Spheroplasts were mounted on poly-L-lysine–coated multiwell slides. Then, slides were submerged in −20°C methanol for 3 min followed by −20°C acetone for 10 s. Next, spheroplasts were incubated with a 1:200 dilution of a rat anti-tubulin antibody (RRID:AB_325005, MCA78G; Bio-Rad) suspended in PBS-BSA (5 mM potassium phosphate, 15 mM NaCl, 1% BSA, and 0.1% sodium azide). After 1–3 h in a wet chamber, primary antibody was removed, and the wells were washed twice with PBS-BSA and incubated with a 1:200 dilution of a preabsorbed anti-rat FITC-conjugated secondary antibody (RRID:AB_2340652, 712-095-153; Jackson ImmunoResearch Labs). After incubation at room temperature for 1 h, antibody was removed, and the wells were washed twice with PBS-BSA. Then, the slide was filled with VectaShield Antifade Mounting Medium with DAPI (Vector Labs) and sealed with a coverslip.

Immunoblotting

To harvest protein, 3.7 OD_{600} equivalents of cells were pelleted and resuspended in 1 ml of 5% TCA and incubated at 4°C for ≥10 min. Then, cells were washed with 1 ml TE50, pH 7.5 (50 mM Tris and 1 mM EDTA), and finally with 1 ml of acetone, and then allowed to dry completely. To extract protein, ~100 µl glass beads and 100 µl lysis buffer (TE50, pH 7.5, 2.75 mM DTT, and 1× cOmplete EDTA-free protease inhibitor cocktail [Roche]) were added to the pellet and shaken with a Mini-Beadbeater-96 (BioSpec). Next, 50 µl of 3× SDS sample buffer (187.5 mM Tris, pH 6.8, 6% 2-mercaptoethanol, 30% glycerol, 9% SDS, and 0.05% bromophenol blue) was added, and the mixture was heated for 5 min. We found that recovery of Num1 was enhanced by heating at 50°C rather than boiling.

Proteins were separated by SDS-PAGE with Bolt 4–12% Bis-Tris Plus Gels (Thermo Fisher Scientific) and transferred onto membranes. For Num1, we transferred to a 0.45-µm Immobilon-FL

PVDF membrane (Li-Cor Biosciences) in a Mini-Protean Tetra tank (Bio-Rad) filled with 25 mM Tris, 192 mM glycine, and 9% methanol, run at 180 mA (maximum, 80 V) for 3 h. For all other blots, we transferred to a 0.45-µm nitrocellulose membrane with a semi-dry transfer system (Trans-Blot Turbo) and its supplied transfer buffer (all from Bio-Rad). Membranes were blocked for 30 min with Odyssey Blocking Buffer (PBS; Li-Cor Biosciences) at room temperature, then incubated overnight at 4°C with primary antibody mixtures diluted in Odyssey Blocking Buffer (PBS) with 0.1% Tween-20. For detection of V5 epitope, we used a mouse anti-V5 antibody (RRID:AB_2556564, R960-25; Thermo Fisher Scientific) at a 1:2,000 dilution. For detection of GFP, we used a mouse anti-GFP antibody (RRID:AB_2313808, 632381; Clontech) at a 1:2,000 dilution. For detection of T7 epitope, we used a mouse anti-T7 antibody (RRID: AB_11211744, 69522; EMD Millipore) at a 1:2,000 dilution. As a loading control, we used a rabbit anti-hexokinase (Hxk2) antibody (RRID:AB_219918, 100-4159; Rockland) at a 1:15,000 dilution. For secondary detection, we used an anti-mouse secondary antibody conjugated to IRDye 800CW at a 1:15,000 dilution (RRID:AB_621847, 926-32212; Li-Cor Biosciences) and an anti-rabbit antibody conjugated to IRDye 680RD at a 1:15,000 dilution (RRID:AB_10956166, 926-68071; Li-Cor Biosciences) in Odyssey Blocking Buffer (PBS) with 0.01% Tween-20. Blots were imaged with an Odyssey CLx scanner (Li-Cor Biosciences), and band intensities were quantified with the Image Studio software associated with the scanner.

Protein purification

Purification of His-tagged Mdm36 was performed as described (Ping et al., 2016) with minor modifications. In brief, 500-ml cultures of Rosetta 2(DE3) *Escherichia coli* (Novagen) bearing expression plasmids and growing in log phase were induced with 250 µM IPTG for 16 h at 18°C. The cells were harvested by centrifugation, and the pellet was resuspended in resuspension buffer (RB; 20 mM Tris, pH 8, 500 mM NaCl, and 1.89 mM 2-mercaptoethanol) and lysed by three freeze-thaw cycles and sonication. Clarified lysates were mixed with one-seventh volume of Ni-NTA agarose (Qiagen) and rotated end-over-end for 1 h at 4°C. Beads were washed in a conical tube with RB, then loaded into a chromatography column and washed with 500 ml of RB plus 30 mM imidazole. Protein was eluted with RB plus 300 mM imidazole, then dialyzed against 20 mM Tris, pH 8, and 500 mM NaCl. Last, glycerol was added to 10%, and proteins were aliquoted and flash-frozen in liquid nitrogen. Protein concentration was estimated by A280.

Ime2-st kinase was purified from yeast (B114), described previously as yDP159 (Phizicky et al., 2018), with minor modifications. Strain B114 contains a pGAL-IME2-st-3xFLAG expression plasmid with a *LEU2* selectable marker. First, a 100-ml culture of SC-Leu with strain B114 was grown overnight with shaking at 30°C. The following day, this culture was used to inoculate 4 liters of YEP+2% glycerol (8× 500-ml cultures in 2-liter baffled flasks) and grown overnight with shaking at 30°C. The following day when the culture reached OD_{600} = 1.2, expression of pGAL-IME2-st-3xFLAG was induced by the addition of galactose to a final concentration of 2%. (The protein contains amino acids 1–404 of Ime2 fused to a 3× FLAG epitope at the C terminus.)

After an additional 6 h of growth, cells were harvested by centrifugation at 4°C.

The yeast pellet was then resuspended in 35 ml lysis buffer (50 mM Hepes, pH 7.6, 10% glycerol, 5 mM Mg-acetate, 1 mM EDTA, 1 mM EGTA, 1 M sorbitol, 0.02% NP-40, 2 mM ATP, 0.5 M KCl, and 1× Halt protease and phosphatase inhibitors), and cells were drop frozen in liquid nitrogen. Frozen cells were lysed under liquid nitrogen in a Waring blender. The resulting powder was thawed and clarified for 1 h at 20,000 rpm at 4°C in a JA-20 rotor (Beckman Coulter). The supernatant was adjusted to 0.3 M KCl and clarified again at 25,000 *g* for 15 min at 4°C.

To isolate the tagged protein, lysate was incubated with 1 ml equilibrated FLAG resin (Sigma) for 2 h with rotation at 4°C. Then, the lysate/resin was transferred to a gravity flow column (at 4°C) and washed with 20 ml H buffer containing 0.3 M KCl and 0.01% NP-40. Beads were washed again with 10 ml H buffer containing 0.3 M KGlut and 0.01% NP-40. Proteins were eluted with 5 ml H buffer containing 0.15 mg/ml 3xFLAG Peptide and 0.3 M KGlut (5× 1-ml elutions incubated for 30 min each). The eluate was subsequently concentrated by ultrafiltration (10-kD molecular weight cutoff; Vivaspin; Vivaproducts) and run through a Superdex 75 column (GE Healthcare) equilibrated with H buffer containing 0.3 M KGlut, 1 mM ATP, and 0.01% NP-40 using a ActaPur FPLC (GE Healthcare). Peak Ime2-st fractions were pooled, aliquoted, and stored at –80°C.

Ime2 IP in vitro kinase assay

Measurement of Ime2 kinase activity in vitro was performed similarly to a published method (Berchowitz et al., 2013). At each time point, cell pellets from 2 ml SPO culture were harvested by centrifugation and snap frozen in liquid nitrogen. Pellets were thawed on ice, and 220 µl NP-40 lysis buffer (50 mM Tris, pH 7.5, 150 mM NaCl, and 1% NP-40) with protease and phosphatase inhibitors (60 mM β-glycerophosphate, 0.1 mM sodium orthovanadate, 15 mM *p*-nitrophenylphosphate, 0.095 U/ml aprotinin [Sigma], 0.1 mg/ml leupeptin [Sigma], 1 mM PMSF [Sigma], 1 mM DTT, and 1× fungal-specific protease inhibitor cocktail [Sigma]) was added. Cells were lysed in a Fast-Prep (MP Bio) with zirconia beads (BioSpec). Lysates were clarified by centrifugation twice at 16,000 *g* for 10 min. Ime2-3V5 IP was performed using 15 µl anti-V5 agarose beads (Sigma) for 2 h at 4°C. IP samples were washed twice with NP-40 lysis buffer, then twice with 25 mM MOPS, pH 7.2.

For kinase reactions, agarose beads with bound Ime2-3V5 were incubated with 6 µl buffer HBII (25 mM MOPS, pH 7.2, 15 mM $MgCl_2$, 5 mM EGTA, 1 mM DTT, 0.02 mg/ml leupeptin, 0.04 U/ml aprotinin, 0.1 mM sodium orthovanadate, and 15 mM *p*-nitrophenylphosphate) for 15 min at room temperature, followed by the addition of 10 µl kinase reaction mixture (25 mM MOPS, pH 7.2, 2 mg/ml Histone H1 [Sigma], and 0.2 mM ATP) containing 50 nCi γ-^{32}P ATP. Kinase reactions were incubated for 15 min at room temperature and stopped by the addition of 10 µl of 3× SDS loading buffer and boiling (5 min). Kinase reactions were separated on a 4–15% SDS Criterion TGX PAGE gel (Bio-Rad) and transferred to a nitrocellulose membrane. The membrane was cut, with the half containing histone H1 subjected to autoradiography (imaged with a Typhoon scanner; GE Healthcare)

and the half containing Ime2-3V5 analyzed by immunoblotting. Ime2 kinase activity was determined by measuring the intensities of the histone H1 autoradiography band for each time point, with the background signal from a no-tag control subtracted. We found measurements of specific activity to be unreliable because of stage-specific differences in intrinsic Ime2 stability.

MECA subunit in vitro kinase assays

Ime2-st kinase and recombinant Mdm36 substrate were purified as described above. Immunoprecipitated substrates were purified as follows. 50 OD_{600} equivalents of cells growing in YPD were pelleted, resuspended in 10 mM Tris, pH 7.5, pelleted again, and flash-frozen in liquid nitrogen. Frozen pellets were thawed on ice and resuspended in 300 µl NP-40 lysis buffer (50 mM Tris, pH 7.5, 150 mM NaCl, 1% NP-40, and 5% glycerol) containing 1 mM DTT, 1 mM EDTA, 3× cOmplete Ultra Protease Inhibitors without EDTA, and 1× PhosSTOP phosphatase inhibitors (Roche). Cells were broken on a Mini-Beadbeater-96, and extracts were clarified by centrifugation at 15,000 g for 15 min. Total protein concentration was determined by Bradford Assay (Bio-Rad). For each IP, 1 mg total protein was incubated with 15 µl V5 agarose beads (Sigma) in a total IP volume of 200 µl. Two parallel IPs were run for each sample. After incubation with extract for 2 h at 4°C, beads were washed with NP-40 lysis buffer supplemented with protease and phosphatase inhibitors. Then, the beads from duplicate IPs were pooled and washed three more times with NP-40 lysis buffer supplemented with inhibitors and twice with 25 mM MOPS. The beads were split for the kinase assay (+Ime2-st and −Ime2-st). Before setting up the kinase assay, half of the bead volumes of each tube were reserved for immunoblot analysis. Proteins were eluted from the beads by incubation in 1× SDS sample buffer (62.5 mM Tris, pH 6.8, 2% 2-mercaptoethanol, 10% glycerol, 3% SDS, and 0.017% bromophenol blue) for 5 min at 50°C.

For the kinase assay, recombinant or on-bead substrate was incubated with 6 µl HBII (15 mM MOPS, 15 mM MgCl$_2$, 5 mM EGTA, 1 mM EDTA, 3× Complete Ultra without EDTA, and 1× PhosSTOP) for 15 min at room temperature. Solution 1 was prepared (1.1 µl of 100 mM ATP, 275 µl water, and 3 µl 6,000 Ci/mmol 10 mCi/ml γ-^{32}P ATP). The kinase reaction was assembled by adding 5 µl solution 1 and 2 µl 1.5 µM Ime2-st to the substrate in HBII, resulting in a final volume of 16 µl in 25 mM MOPS. After 15 min at room temperature, reactions were stopped with 3× SDS sample buffer, heated, and run on an SDS-PAGE gel. The gels were fixed in 10% methanol and 10% acetic acid, dried, and exposed to a phosphor screen. Screens were imaged with a Typhoon scanner (GE Healthcare).

Denaturing IP and MS

To generate denatured protein extracts, cells were first pelleted in multiples of 9.25 OD_{600} equivalents (i.e., 5 ml SPO culture), then resuspended in two-fifths culture volume of 5% TCA at 4°C and distributed into tubes such that each contained 9.25 OD_{600} equivalents. After incubation overnight at 4°C, cells were pelleted, washed once with acetone, and dried completely. To break pellets, 100 µl zirconia beads and 150 µl TE50, pH 7.5, 2.75 mM DTT, 1× PhosSTOP (Roche), and 3× cOmplete Ultra EDTA Free (Roche) were added to each tube. Pellets were disrupted on a Mini-Beadbeater-96. SDS was added to 1%, extracts were denatured by heating at 50°C for 5 min, and NP-40 lysis buffer (50 mM Tris, pH 7.5, 150 mM NaCl, 1% NP-40, and 5% glycerol) was added, supplemented with 1× PhosSTOP and 3× cOmplete Ultra EDTA Free, to a final volume of 1.5 ml (i.e., diluting SDS to 0.1%). Cleared lysates pooled from five tubes were added to V5 agarose beads (Sigma), incubated for 2 h at 4°C with rotation, and then washed twice with each of the following: (1) 50 mM Tris, pH 7.5, 1 M NaCl, 1 mM EDTA, and 1% NP-40; (2) 50 mM Tris, pH 7.5, 150 mM NaCl, 10 mM MgCl$_2$, 0.05% NP-40, and 5% glycerol; and (3) 50 mM Tris, pH 7.5, 150 mM NaCl, 10 mM MgCl$_2$, and 5% glycerol. After washes, 1× SDS sample buffer was added to the beads, and proteins were eluted by heating at 50°C for 5 min. Eluted proteins were separated by SDS-PAGE, then stained with a Colloidal Blue Staining Kit (Invitrogen).

Gel bands containing the desired protein were excised, washed for 20 min in 500 µl of 100 mM NH$_4$HCO$_3$, then incubated at 50°C for 15 min in 150 µl of 100 mM NH$_4$HCO$_3$ and 2.8 mM DTT. 10 µl of 100 mM iodoacetamide was then added to the cooled gel band mixtures and incubated for 15 min in the dark at room temperature. Then the gel slice was washed in 500 µl of equal parts 100 mM NH$_4$HCO$_3$ and acetonitrile with shaking for 20 min. Gel slices were shrunk by soaking in 50 µl acetonitrile for 15 min. Then the supernatant was removed, and residual solvent was removed in a speed vac. Gel fragments were rehydrated with 10 µl of 25 mM NH$_4$HCO$_3$ containing sequencing-grade modified trypsin (Promega), incubated at room temperature for 15 min, and then supplemented with additional trypsin to completely cover the gel slices. Digestion was allowed to continue overnight at 37°C. Then, the supernatant, with two washes with 60% acetonitrile and 0.1% formic acid and one wash with acetonitrile were all combined and dried completely in a SpeedVac.

MS was performed by the Vincent J. Coates Proteomics/Mass Spectrometry Laboratory at University of California, Berkeley. mudPIT methods were used to achieve good sequence coverage of target proteins in a complex mixture. A nano LC column was packed in a 100-µm inner-diameter glass capillary with an emitter tip. The column consisted of 10 cm of Polaris c18 5 µm packing material (Varian), followed by 4 cm of Partisphere 5 SCX (Whatman). The column was loaded by use of a pressure bomb and washed extensively with buffer A (see below). The column was then directly coupled to an electrospray ionization source mounted on a LTQ XL linear ion trap mass spectrometer (Thermo Fisher Scientific). An Agilent 1200 HPLC equipped with a split line to deliver a flow rate of 300 nl/min was used for chromatography. Peptides were eluted using an eight-step mudPIT procedure (Washburn et al., 2001). Buffer A was 5% acetonitrile and 0.02% heptafluorobutyric acid (HFBA). Buffer B was 80% acetonitrile and 0.02% HFBA. Buffer C was 250 mM ammonium acetate, 5% acetonitrile, and 0.02% HFBA. Buffer D was the same as buffer C, but with 500 mM ammonium acetate.

Protein identification was performed with Integrated Proteomics Pipeline (IP2; Integrated Proteomics Applications) using ProLuCID/Sequest, DTASelect2, and Census (Tabb et al., 2002; Cociorva et al., 2007; Park et al., 2008; Xu et al., 2015). Tandem mass spectra were extracted into ms1 and ms2 files from raw files by using RawExtractor (McDonald et al., 2004). Data were

searched against the SK1 sequence of the target protein (Yue et al., 2017) plus the yeast database supplemented with sequences of common contaminants and concatenated to a decoy database in which the sequence for each entry in the original database was reversed (Peng et al., 2003). LTQ data were searched with 3,000.0 milli-atomic mass unit precursor tolerance, and the fragment ions were restricted to a 600.0 parts per million tolerance. All searches were parallelized and searched on the Vincent J. Coates proteomics cluster. Search space included all fully tryptic peptide candidates with no missed cleavage restrictions. Carbamidomethylation (+57.02146) of cysteine was considered a static modification. We required 1 peptide per protein and both tryptic termini for each protein identification. The ProLuCID search results were assembled and filtered using the DTASelect program (Tabb et al., 2002; Cociorva et al., 2007) with a peptide false discovery rate (FDR) of 0.001 for single peptides and a peptide FDR of 0.005 for additional peptides for the same protein. Under such filtering conditions, the estimated FDR for peptides was never more than 0.5%. Spectra for individual posttranslational modifications of interest were manually inspected.

Data availability
All the reagents generated in this study are available upon request.

Online supplemental material
Video 1 shows the Htb1-mCherry marker strain undergoing meiosis; Video 2, the GFP-Spo20[51–91] marker strain; and Video 3, the Spc42-GFP strain. Videos 4 and 5 show *pGAL-NDT80* (± *GAL* induction) cells undergoing meiosis or arrested in prophase I. Videos 6 and 7 show *ime2-as1* and control cells undergoing meiosis. Fig. S1 contains montages of Videos 4–7. Fig. S2 shows that *CDC20* is not necessary for Num1 degradation and that the *rpn6-1* allele phenocopies MG-132 treatment. Fig. S3 shows that the *MDM36-3V5* allele is functional. Table S1 lists the strains used in this study. Table S2 lists the plasmids used.

Acknowledgments

References

Anand, R., G. Memisoglu, and J. Haber. 2017. Cas9-mediated gene editing in Saccharomyces cerevisiae. *Protocol Exchange*. https://doi.org/10.1083/protex.2017.021a

Benjamin, K.R., C. Zhang, K.M. Shokat, and I. Herskowitz. 2003. Control of landmark events in meiosis by the CDK Cdc28 and the meiosis-specific kinase Ime2. *Genes Dev.* 17:1524–1539. https://doi.org/10.1101/gad.1101503

Berchowitz, L.E., A.S. Gajadhar, F.J. van Werven, A.A. De Rosa, M.L. Samoylova, G.A. Brar, Y. Xu, C. Xiao, B. Futcher, J.S. Weissman, et al. 2013. A developmentally regulated translational control pathway establishes the meiotic chromosome segregation pattern. *Genes Dev.* 27:2147–2163. https://doi.org/10.1101/gad.224253.113

Berchowitz, L.E., G. Kabachinski, M.R. Walker, T.M. Carlile, W.V. Gilbert, T.U. Schwartz, and A. Amon. 2015. Regulated formation of an amyloid-like translational repressor governs gametogenesis. *Cell.* 163:406–418. https://doi.org/10.1016/j.cell.2015.08.060

Bishop, A.C., J.A. Ubersax, D.T. Petsch, D.P. Matheos, N.S. Gray, J. Blethrow, E. Shimizu, J.Z. Tsien, P.G. Schultz, M.D. Rose, et al. 2000. A chemical switch for inhibitor-sensitive alleles of any protein kinase. *Nature.* 407:395–401. https://doi.org/10.1038/35030148

Bohnert, K.A., and C. Kenyon. 2017. A lysosomal switch triggers proteostasis renewal in the immortal C. elegans germ lineage. *Nature.* 551:629–633.

Brar, G.A., M. Yassour, N. Friedman, A. Regev, N.T. Ingolia, and J.S. Weissman. 2012. High-resolution view of the yeast meiotic program revealed by ribosome profiling. *Science.* 335:552–557. https://doi.org/10.1126/science.1215110

Brewer, B.J., and W.L. Fangman. 1980. Preferential inclusion of extrachromosomal genetic elements in yeast meiotic spores. *Proc. Natl. Acad. Sci. USA.* 77:5380–5384. https://doi.org/10.1073/pnas.77.9.5380

Carlile, T.M., and A. Amon. 2008. Meiosis I is established through division-specific translational control of a cyclin. *Cell.* 133:280–291. https://doi.org/10.1016/j.cell.2008.02.032

Carpenter, K., R.B. Bell, J. Yunus, A. Amon, and L.E. Berchowitz. 2018. Phosphorylation-mediated clearance of amyloid-like assemblies in meiosis. *Dev. Cell.* 45:392–405.e6. https://doi.org/10.1016/j.devcel.2018.04.001

Cerveny, K.L., S.L. Studer, R.E. Jensen, and H. Sesaki. 2007. Yeast mitochondrial division and distribution require the cortical num1 protein. *Dev. Cell.* 12:363–375. https://doi.org/10.1016/j.devcel.2007.01.017

Cheng, Z., G.M. Otto, E.N. Powers, A. Keskin, P. Mertins, S.A. Carr, M. Jovanovic, and G.A. Brar. 2018. Pervasive, coordinated protein-level changes driven by transcript isoform switching during meiosis. *Cell.* 172:910–923.e16. https://doi.org/10.1016/j.cell.2018.01.035

Christianson, T.W., R.S. Sikorski, M. Dante, J.H. Shero, and P. Hieter. 1992. Multifunctional yeast high-copy-number shuttle vectors. *Gene.* 110:119–122. https://doi.org/10.1016/0378-1119(92)90454-W

Chu, S., and I. Herskowitz. 1998. Gametogenesis in yeast is regulated by a transcriptional cascade dependent on Ndt80. *Mol. Cell.* 1:685–696. https://doi.org/10.1016/S1097-2765(00)80068-4

Chu, J., R.D. Haynes, S.Y. Corbel, P. Li, E. González-González, J.S. Burg, N.J. Ataie, A.J. Lam, P.J. Cranfill, M.A. Baird, et al. 2014. Non-invasive intravital imaging of cellular differentiation with a bright red-excitable fluorescent protein. *Nat. Methods.* 11:572–578. https://doi.org/10.1038/nmeth.2888

Cociorva, D., D.L. Tabb, and J.R. Yates. 2007. Validation of tandem mass spectrometry database search results using DTASelect. Curr. Protoc. Bioinformatics. Chapter 13:Unit 13 14.

Cooper, K.F., M.J. Mallory, D.B. Egeland, M. Jarnik, and R. Strich. 2000. Ama1p is a meiosis-specific regulator of the anaphase promoting complex/cyclosome in yeast. Proc. Natl. Acad. Sci. USA. 97:14548–14553. https://doi.org/10.1073/pnas.250351297

Cox, R.T., and A.C. Spradling. 2003. A Balbiani body and the fusome mediate mitochondrial inheritance during Drosophila oogenesis. Development. 130:1579–1590. https://doi.org/10.1242/dev.00365

DeLuca, S.Z., and P.H. O'Farrell. 2012. Barriers to male transmission of mitochondrial DNA in sperm development. Dev. Cell. 22:660–668. https://doi.org/10.1016/j.devcel.2011.12.021

Diamond, A.E., J.S. Park, I. Inoue, H. Tachikawa, and A.M. Neiman. 2009. The anaphase promoting complex targeting subunit Ama1 links meiotic exit to cytokinesis during sporulation in Saccharomyces cerevisiae. Mol. Biol. Cell. 20:134–145. https://doi.org/10.1091/mbc.e08-06-0615

Dirick, L., L. Goetsch, G. Ammerer, and B. Byers. 1998. Regulation of meiotic S phase by Ime2 and a Clb5,6-associated kinase in Saccharomyces cerevisiae. Science. 281:1854–1857. https://doi.org/10.1126/science.281.5384.1854

Eastwood, M.D., and M.D. Meneghini. 2015. Developmental coordination of gamete differentiation with programmed cell death in sporulating yeast. Eukaryot. Cell. 14:858–867. https://doi.org/10.1128/EC.00068-15

Eastwood, M.D., S.W. Cheung, K.Y. Lee, J. Moffat, and M.D. Meneghini. 2012. Developmentally programmed nuclear destruction during yeast gametogenesis. Dev. Cell. 23:35–44. https://doi.org/10.1016/j.devcel.2012.05.005

Eisenberg-Bord, M., N. Shai, M. Schuldiner, and M. Bohnert. 2016. A tether is a tether is a tether: tethering at membrane contact sites. Dev. Cell. 39:395–409. https://doi.org/10.1016/j.devcel.2016.10.022

Elbaz-Alon, Y., E. Rosenfeld-Gur, V. Shinder, A.H. Futerman, T. Geiger, and M. Schuldiner. 2014. A dynamic interface between vacuoles and mitochondria in yeast. Dev. Cell. 30:95–102. https://doi.org/10.1016/j.devcel.2014.06.007

Elbaz-Alon, Y., M. Eisenberg-Bord, V. Shinder, S.B. Stiller, E. Shimoni, N. Wiedemann, T. Geiger, and M. Schuldiner. 2015. Lam6 regulates the extent of contacts between organelles. Cell Reports. 12:7–14. https://doi.org/10.1016/j.celrep.2015.06.022

Foiani, M., E. Nadjar-Boger, R. Capone, S. Sagee, T. Hashimshoni, and Y. Kassir. 1996. A meiosis-specific protein kinase, Ime2, is required for the correct timing of DNA replication and for spore formation in yeast meiosis. Mol. Gen. Genet. 253:278–288. https://doi.org/10.1007/s004380050323

Friedman, J.R., and J. Nunnari. 2014. Mitochondrial form and function. Nature. 505:335–343. https://doi.org/10.1038/nature12985

Fuchs, J., and J. Loidl. 2004. Behaviour of nucleolus organizing regions (NORs) and nucleoli during mitotic and meiotic divisions in budding yeast. Chromosome Res. 12:427–438. https://doi.org/10.1023/B:CHRO.0000034726.05374.db

Gorsich, S.W., and J.M. Shaw. 2004. Importance of mitochondrial dynamics during meiosis and sporulation. Mol. Biol. Cell. 15:4369–4381. https://doi.org/10.1091/mbc.e03-12-0875

Goudeau, J., and H. Aguilaniu. 2010. Carbonylated proteins are eliminated during reproduction in C. elegans. Aging Cell. 9:991–1003. https://doi.org/10.1111/j.1474-9726.2010.00625.x

Graef, M., J.R. Friedman, C. Graham, M. Babu, and J. Nunnari. 2013. ER exit sites are physical and functional core autophagosome biogenesis components. Mol. Biol. Cell. 24:2918–2931. https://doi.org/10.1091/mbc.e13-07-0381

Helle, S.C., G. Kanfer, K. Kolar, A. Lang, A.H. Michel, and B. Kornmann. 2013. Organization and function of membrane contact sites. Biochim. Biophys. Acta. 1833:2526–2541. https://doi.org/10.1016/j.bbamcr.2013.01.028

Hepworth, S.R., H. Friesen, and J. Segall. 1998. NDT80 and the meiotic recombination checkpoint regulate expression of middle sporulation-specific genes in Saccharomyces cerevisiae. Mol. Cell. Biol. 18:5750–5761. https://doi.org/10.1128/MCB.18.10.5750

Higuchi-Sanabria, R., T.C. Swayne, I.R. Boldogh, and L.A. Pon. 2016. Live-cell imaging of mitochondria and the actin cytoskeleton in budding yeast. Methods Mol. Biol. 1365:25–62. https://doi.org/10.1007/978-1-4939-3124-8_2

Hoffmann, H.P., and C.J. Avers. 1973. Mitochondrion of yeast: ultrastructural evidence for one giant, branched organelle per cell. Science. 181:749–751. https://doi.org/10.1126/science.181.4101.749

Hönscher, C., M. Mari, K. Auffarth, M. Bohnert, J. Griffith, W. Geerts, M. van der Laan, M. Cabrera, F. Reggiori, and C. Ungermann. 2014. Cellular metabolism regulates contact sites between vacuoles and mitochondria. Dev. Cell. 30:86–94. https://doi.org/10.1016/j.devcel.2014.06.006

Hurd, T.R., B. Herrmann, J. Sauerwald, J. Sanny, M. Grosch, and R. Lehmann. 2016. Long oskar controls mitochondrial inheritance in Drosophila melanogaster. Dev. Cell. 39:560–571. https://doi.org/10.1016/j.devcel.2016.11.004

Irniger, S. 2011. The Ime2 protein kinase family in fungi: more duties than just meiosis. Mol. Microbiol. 80:1–13. https://doi.org/10.1111/j.1365-2958.2011.07575.x

Isono, E., N. Saito, N. Kamata, Y. Saeki, and A. Toh-E. 2005. Functional analysis of Rpn6p, a lid component of the 26 S proteasome, using temperature-sensitive rpn6 mutants of the yeast Saccharomyces cerevisiae. J. Biol. Chem. 280:6537–6547. https://doi.org/10.1074/jbc.M409364200

Janke, C., M.M. Magiera, N. Rathfelder, C. Taxis, S. Reber, H. Maekawa, A. Moreno-Borchart, G. Doenges, E. Schwob, E. Schiebel, and M. Knop. 2004. A versatile toolbox for PCR-based tagging of yeast genes: new fluorescent proteins, more markers and promoter substitution cassettes. Yeast. 21:947–962. https://doi.org/10.1002/yea.1142

Kahana, J.A., B.J. Schnapp, and P.A. Silver. 1995. Kinetics of spindle pole body separation in budding yeast. Proc. Natl. Acad. Sci. USA. 92:9707–9711. https://doi.org/10.1073/pnas.92.21.9707

Kamieniecki, R.J., L. Liu, and D.S. Dawson. 2005. FEAR but not MEN genes are required for exit from meiosis I. Cell Cycle. 4:4093–4098. https://doi.org/10.4161/cc.4.8.1857

Kanki, T., and D.J. Klionsky. 2008. Mitophagy in yeast occurs through a selective mechanism. J. Biol. Chem. 283:32386–32393. https://doi.org/10.1074/jbc.M802403200

Klapholz, S., and R.E. Esposito. 1980. Isolation of SPO12-1 and SPO13-1 from a natural variant of yeast that undergoes a single meiotic division. Genetics. 96:567–588.

Klecker, T., D. Scholz, J. Förtsch, and B. Westermann. 2013. The yeast cell cortical protein Num1 integrates mitochondrial dynamics into cellular architecture. J. Cell Sci. 126:2924–2930. https://doi.org/10.1242/jcs.126045

Kloc, M., S. Bilinski, and L.D. Etkin. 2004. The Balbiani body and germ cell determinants: 150 years later. Curr. Top. Dev. Biol. 59:1–36. https://doi.org/10.1016/S0070-2153(04)59001-4

Knop, M., and K. Strasser. 2000. Role of the spindle pole body of yeast in mediating assembly of the prospore membrane during meiosis. EMBO J. 19:3657–3667. https://doi.org/10.1093/emboj/19.14.3657

Kominami, K., Y. Sakata, M. Sakai, and I. Yamashita. 1993. Protein kinase activity associated with the IME2 gene product, a meiotic inducer in the yeast Saccharomyces cerevisiae. Biosci. Biotechnol. Biochem. 57:1731–1735. https://doi.org/10.1271/bbb.57.1731

Kornmann, B., E. Currie, S.R. Collins, M. Schuldiner, J. Nunnari, J.S. Weissman, and P. Walter. 2009. An ER-mitochondria tethering complex revealed by a synthetic biology screen. Science. 325:477–481. https://doi.org/10.1126/science.1175088

Kraft, L.M., and L.L. Lackner. 2017. Mitochondria-driven assembly of a cortical anchor for mitochondria and dynein. J. Cell Biol. 216:3061–3071. https://doi.org/10.1083/jcb.201702022

Kraft, L.M., and L.L. Lackner. 2018. Mitochondrial anchors: Positioning mitochondria and more. Biochem. Biophys. Res. Commun. 500:2–8. https://doi.org/10.1016/j.bbrc.2017.06.193

Kumagai, K., M. Kawano-Kawada, and K. Hanada. 2014. Phosphoregulation of the ceramide transport protein CERT at serine 315 in the interaction with VAMP-associated protein (VAP) for inter-organelle trafficking of ceramide in mammalian cells. J. Biol. Chem. 289:10748–10760. https://doi.org/10.1074/jbc.M113.528380

Lackner, L.L., H. Ping, M. Graef, A. Murley, and J. Nunnari. 2013. Endoplasmic reticulum-associated mitochondria-cortex tether functions in the distribution and inheritance of mitochondria. Proc. Natl. Acad. Sci. USA. 110:E458–E467. https://doi.org/10.1073/pnas.1215232110

Lee, B.H., and A. Amon. 2003. Role of Polo-like kinase CDC5 in programming meiosis I chromosome segregation. Science. 300:482–486. https://doi.org/10.1126/science.1081846

Longtine, M.S., A. McKenzie III, D.J. Demarini, N.G. Shah, A. Wach, A. Brachat, P. Philippsen, and J.R. Pringle. 1998. Additional modules for versatile and economical PCR-based gene deletion and modification in Saccharomyces cerevisiae. Yeast. 14:953–961. https://doi.org/10.1002/(SICI)1097-0061(199807)14:10%3C953::AID-YEA293%3E3.0.CO;2-U

Manford, A.G., C.J. Stefan, H.L. Yuan, J.A. Macgurn, and S.D. Emr. 2012. ER-to-plasma membrane tethering proteins regulate cell signaling and ER morphology. Dev. Cell. 23:1129–1140. https://doi.org/10.1016/j.devcel.2012.11.004

Marston, A.L., and A. Amon. 2004. Meiosis: cell-cycle controls shuffle and deal. *Nat. Rev. Mol. Cell Biol.* 5:983–997. https://doi.org/10.1038/nrm1526

Marston, A.L., B.H. Lee, and A. Amon. 2003. The Cdc14 phosphatase and the FEAR network control meiotic spindle disassembly and chromosome segregation. *Dev. Cell.* 4:711–726. https://doi.org/10.1016/S1534-5807(03)00130-8

McDonald, W.H., D.L. Tabb, R.G. Sadygov, M.J. MacCoss, J. Venable, J. Graumann, J.R. Johnson, D. Cociorva, and J.R. Yates III. 2004. MS1, MS2, and SQT-three unified, compact, and easily parsed file formats for the storage of shotgun proteomic spectra and identifications. *Rapid Commun. Mass Spectrom.* 18:2162–2168. https://doi.org/10.1002/rcm.1603

Mishra, P., and D.C. Chan. 2014. Mitochondrial dynamics and inheritance during cell division, development and disease. *Nat. Rev. Mol. Cell Biol.* 15:634–646. https://doi.org/10.1038/nrm3877

Miyakawa, I., H. Aoi, N. Sando, and T. Kuroiwa. 1984. Fluorescence microscopic studies of mitochondrial nucleoids during meiosis and sporulation in the yeast, Saccharomyces cerevisiae. *J. Cell Sci.* 66:21–38.

Murley, A., and J. Nunnari. 2016. The emerging network of mitochondria-organelle contacts. *Mol. Cell.* 61:648–653. https://doi.org/10.1016/j.molcel.2016.01.031

Murley, A., L.L. Lackner, C. Osman, M. West, G.K. Voeltz, P. Walter, and J. Nunnari. 2013. ER-associated mitochondrial division links the distribution of mitochondria and mitochondrial DNA in yeast. *eLife.* 2:e00422. https://doi.org/10.7554/eLife.00422

Murley, A., R.D. Sarsam, A. Toulmay, J. Yamada, W.A. Prinz, and J. Nunnari. 2015. Ltc1 is an ER-localized sterol transporter and a component of ER-mitochondria and ER-vacuole contacts. *J. Cell Biol.* 209:539–548. https://doi.org/10.1083/jcb.201502033

Nakanishi, H., P. de los Santos, and A.M. Neiman. 2004. Positive and negative regulation of a SNARE protein by control of intracellular localization. *Mol. Biol. Cell.* 15:1802–1815. https://doi.org/10.1091/mbc.e03-11-0798

Neiman, A.M. 1998. Prospore membrane formation defines a developmentally regulated branch of the secretory pathway in yeast. *J. Cell Biol.* 140:29–37. https://doi.org/10.1083/jcb.140.1.29

Neiman, A.M. 2011. Sporulation in the budding yeast Saccharomyces cerevisiae. *Genetics.* 189:737–765. https://doi.org/10.1534/genetics.111.127126

Nhek, S., M. Ngo, X. Yang, M.M. Ng, S.J. Field, J.M. Asara, N.D. Ridgway, and A. Toker. 2010. Regulation of oxysterol-binding protein Golgi localization through protein kinase D-mediated phosphorylation. *Mol. Biol. Cell.* 21:2327–2337. https://doi.org/10.1091/mbc.e10-02-0090

Nishimura, K., T. Fukagawa, H. Takisawa, T. Kakimoto, and M. Kanemaki. 2009. An auxin-based degron system for the rapid depletion of proteins in nonplant cells. *Nat. Methods.* 6:917–922. https://doi.org/10.1038/nmeth.1401

Nocedal, I., E. Mancera, and A.D. Johnson. 2017. Gene regulatory network plasticity predates a switch in function of a conserved transcription regulator. *eLife.* 6:e23250. https://doi.org/10.7554/eLife.23250

Nunnari, J., W.F. Marshall, A. Straight, A. Murray, J.W. Sedat, and P. Walter. 1997. Mitochondrial transmission during mating in Saccharomyces cerevisiae is determined by mitochondrial fusion and fission and the intramitochondrial segregation of mitochondrial DNA. *Mol. Biol. Cell.* 8:1233–1242. https://doi.org/10.1091/mbc.8.7.1233

Omer, S., S.R. Greenberg, and W.L. Lee. 2018. Cortical dynein pulling mechanism is regulated by differentially targeted attachment molecule Num1. *eLife.* 7:e36745. https://doi.org/10.7554/eLife.36745

Padmore, R., L. Cao, and N. Kleckner. 1991. Temporal comparison of recombination and synaptonemal complex formation during meiosis in S. cerevisiae. *Cell.* 66:1239–1256. https://doi.org/10.1016/0092-8674(91)90046-2

Palmer, R.E., M. Koval, and D. Koshland. 1989. The dynamics of chromosome movement in the budding yeast Saccharomyces cerevisiae. *J. Cell Biol.* 109:3355–3366. https://doi.org/10.1083/jcb.109.6.3355

Park, S.K., J.D. Venable, T. Xu, and J.R. Yates III. 2008. A quantitative analysis software tool for mass spectrometry-based proteomics. *Nat. Methods.* 5:319–322. https://doi.org/10.1038/nmeth.1195

Peng, J., J.E. Elias, C.C. Thoreen, L.J. Licklider, and S.P. Gygi. 2003. Evaluation of multidimensional chromatography coupled with tandem mass spectrometry (LC/LC-MS/MS) for large-scale protein analysis: the yeast proteome. *J. Proteome Res.* 2:43–50. https://doi.org/10.1021/pr025556v

Phizicky, D.V., L.E. Berchowitz, and S.P. Bell. 2018. Multiple kinases inhibit origin licensing and helicase activation to ensure reductive cell division during meiosis. *eLife.* 7:e33309. https://doi.org/10.7554/eLife.33309

Ping, H.A., L.M. Kraft, W. Chen, A.E. Nilles, and L.L. Lackner. 2016. Num1 anchors mitochondria to the plasma membrane via two domains with different lipid binding specificities. *J. Cell Biol.* 213:513–524. https://doi.org/10.1083/jcb.201511021

Prinz, W.A. 2014. Bridging the gap: membrane contact sites in signaling, metabolism, and organelle dynamics. *J. Cell Biol.* 205:759–769. https://doi.org/10.1083/jcb.201401126

Rojansky, R., M.Y. Cha, and D.C. Chan. 2016. Elimination of paternal mitochondria in mouse embryos occurs through autophagic degradation dependent on PARKIN and MUL1. *eLife.* 5:e17896. https://doi.org/10.7554/eLife.17896

Rudge, S.A., V.A. Sciorra, M. Iwamoto, C. Zhou, T. Strahl, A.J. Morris, J. Thorner, and J. Engebrecht. 2004. Roles of phosphoinositides and of Spo14p (phospholipase D)-generated phosphatidic acid during yeast sporulation. *Mol. Biol. Cell.* 15:207–218. https://doi.org/10.1091/mbc.e03-04-0245

Schindelin, J., I. Arganda-Carreras, E. Frise, V. Kaynig, M. Longair, T. Pietzsch, S. Preibisch, C. Rueden, S. Saalfeld, B. Schmid, et al. 2012. Fiji: an open-source platform for biological-image analysis. *Nat. Methods.* 9:676–682. https://doi.org/10.1038/nmeth.2019

Schrader, M., L.F. Godinho, J.L. Costello, and M. Islinger. 2015. The different facets of organelle interplay-an overview of organelle interactions. *Front. Cell Dev. Biol.* 3:56. https://doi.org/10.3389/fcell.2015.00056

Sheff, M.A., and K.S. Thorn. 2004. Optimized cassettes for fluorescent protein tagging in Saccharomyces cerevisiae. *Yeast.* 21:661–670. https://doi.org/10.1002/yea.1130

Sia, R.A., and A.P. Mitchell. 1995. Stimulation of later functions of the yeast meiotic protein kinase Ime2p by the IDS2 gene product. *Mol. Cell. Biol.* 15:5279–5287. https://doi.org/10.1128/MCB.15.10.5279

Smith, H.E., and A.P. Mitchell. 1989. A transcriptional cascade governs entry into meiosis in Saccharomyces cerevisiae. *Mol. Cell. Biol.* 9:2142–2152. https://doi.org/10.1128/MCB.9.5.2142

Sopko, R., S. Raithatha, and D. Stuart. 2002. Phosphorylation and maximal activity of Saccharomyces cerevisiae meiosis-specific transcription factor Ndt80 is dependent on Ime2. *Mol. Cell. Biol.* 22:7024–7040. https://doi.org/10.1128/MCB.22.20.7024-7040.2002

Stegmeier, F., R. Visintin, and A. Amon. 2002. Separase, polo kinase, the kinetochore protein Slk19, and Spo12 function in a network that controls Cdc14 localization during early anaphase. *Cell.* 108:207–220. https://doi.org/10.1016/S0092-8674(02)00618-9

Stevens, B. 1981. Mitochondrial Structure. *In* The Molecular Biology of the Yeast Saccharomyces: Life Cycle and Inheritance. Vol. 11A. E.W. Strathern, and J.R. Broach, editors. Cold Spring Harbor Laboratory Press, New York. 471–504.

Suda, Y., H. Nakanishi, E.M. Mathieson, and A.M. Neiman. 2007. Alternative modes of organellar segregation during sporulation in Saccharomyces cerevisiae. *Eukaryot. Cell.* 6:2009–2017. https://doi.org/10.1128/EC.00238-07

Tabb, D.L., W.H. McDonald, and J.R. Yates III. 2002. DTASelect and Contrast: tools for assembling and comparing protein identifications from shotgun proteomics. *J. Proteome Res.* 1:21–26. https://doi.org/10.1021/pr015504q

Tang, X., B.S. Germain, and W.L. Lee. 2012. A novel patch assembly domain in Num1 mediates dynein anchoring at the cortex during spindle positioning. *J. Cell Biol.* 196:743–756. https://doi.org/10.1083/jcb.201112017

Tsai, I.T., J.L. Lin, Y.H. Chiang, Y.C. Chuang, S.S. Liang, C.N. Chuang, T.N. Huang, and T.F. Wang. 2014. Interorganelle interactions and inheritance patterns of nuclei and vacuoles in budding yeast meiosis. *Autophagy.* 10:285–295. https://doi.org/10.4161/auto.27192

Tung, K.S., E.J. Hong, and G.S. Roeder. 2000. The pachytene checkpoint prevents accumulation and phosphorylation of the meiosis-specific transcription factor Ndt80. *Proc. Natl. Acad. Sci. USA.* 97:12187–12192. https://doi.org/10.1073/pnas.220464597

Unal, E., B. Kinde, and A. Amon. 2011. Gametogenesis eliminates age-induced cellular damage and resets life span in yeast. *Science.* 332:1554–1557. https://doi.org/10.1126/science.1204349

van Werven, F.J., and A. Amon. 2011. Regulation of entry into gametogenesis. *Philos. Trans. R. Soc. Lond. B Biol. Sci.* 366:3521–3531. https://doi.org/10.1098/rstb.2011.0081

Wang, Y., C.Y. Chang, J.F. Wu, and K.S. Tung. 2011. Nuclear localization of the meiosis-specific transcription factor Ndt80 is regulated by the pachytene checkpoint. *Mol. Biol. Cell.* 22:1878–1886. https://doi.org/10.1091/mbc.e10-12-1011

Washburn, M.P., D. Wolters, and J.R. Yates III. 2001. Large-scale analysis of the yeast proteome by multidimensional protein identification technology. *Nat. Biotechnol.* 19:242–247. https://doi.org/10.1038/85686

Westermann, B. 2014. Mitochondrial inheritance in yeast. *Biochim. Biophys. Acta.* 1837:1039–1046. https://doi.org/10.1016/j.bbabio.2013.10.005

Winter, E. 2012. The Sum1/Ndt80 transcriptional switch and commitment to meiosis in Saccharomyces cerevisiae. *Microbiol. Mol. Biol. Rev.* 76:1–15. https://doi.org/10.1128/MMBR.05010-11

Xu, L., M. Ajimura, R. Padmore, C. Klein, and N. Kleckner. 1995. NDT80, a meiosis-specific gene required for exit from pachytene in Saccharomyces cerevisiae. *Mol. Cell. Biol.* 15:6572–6581. https://doi.org/10.1128/MCB.15.12.6572

Xu, T., S.K. Park, J.D. Venable, J.A. Wohlschlegel, J.K. Diedrich, D. Cociorva, B. Lu, L. Liao, J. Hewel, X. Han, et al. 2015. ProLuCID: An improved SEQ UEST-like algorithm with enhanced sensitivity and specificity. *J. Proteomics.* 129:16–24. https://doi.org/10.1016/j.jprot.2015.07.001

Yeh, E., R.V. Skibbens, J.W. Cheng, E.D. Salmon, and K. Bloom. 1995. Spindle dynamics and cell cycle regulation of dynein in the budding yeast, Saccharomyces cerevisiae. *J. Cell Biol.* 130:687–700. https://doi.org/10.1083/jcb.130.3.687

Yoshida, M., H. Kawaguchi, Y. Sakata, K. Kominami, M. Hirano, H. Shima, R. Akada, and I. Yamashita. 1990. Initiation of meiosis and sporulation in Saccharomyces cerevisiae requires a novel protein kinase homologue. *Mol. Gen. Genet.* 221:176–186. https://doi.org/10.1007/BF00261718

Yoshida, S., K. Asakawa, and A. Toh-e. 2002. Mitotic exit network controls the localization of Cdc14 to the spindle pole body in Saccharomyces cerevisiae. *Curr. Biol.* 12:944–950. https://doi.org/10.1016/S0960-9822(02)00870-9

Youk, H., and W.A. Lim. 2014. Secreting and sensing the same molecule allows cells to achieve versatile social behaviors. *Science.* 343:1242782. https://doi.org/10.1126/science.1242782

Yue, J.X., J. Li, L. Aigrain, J. Hallin, K. Persson, K. Oliver, A. Bergström, P. Coupland, J. Warringer, M.C. Lagomarsino, et al. 2017. Contrasting evolutionary genome dynamics between domesticated and wild yeasts. *Nat. Genet.* 49:913–924. https://doi.org/10.1038/ng.3847